# Life history diversity in a large group of chloroviruses

Eva J.P. Lievens[1,*], Irina V. Agarkova[2,3], David D. Dunigan[2,3], James L. Van Etten[2,3], and Lutz Becks[1]

[1]Aquatic Ecology and Evolution Group, Limnological Institute, University of Konstanz, Mainaustraße 252, 78464 Konstanz, Germany

[2]Department of Plant Pathology, University of Nebraska-Lincoln, Lincoln, NE USA 68583-xxxx

[3]Nebraska Center for Virology, University of Nebraska-Lincoln, Lincoln, NE USA 68583-0900

*eva.j.lievens@gmail.com

**Abstract**

Life history traits shape the evolution and ecology of microbial viruses through their effects on epidemiology, their diversity, and the trade-offs between them. However, our understanding of their diversity is hampered by the difficulty of isolating and phenotyping large numbers of related viruses. In this study, we overcame these challenges to describe the life history diversity of the genus *Chlorovirus*, which contains lytic dsDNA viruses that infect unicellular green algae. We developed efficient methods to measure adsorption rate, depolarization probability, lysis completion probability, lysis time, burst size, specific infectivity, and mortality rate. We used these methods to quantify the life history traits of 35 chlorovirus strains from three host range groups (NC64A, Osy, and SAG viruses). The viruses were highly diverse: trait estimates varied by a factor of 5 to 75 across all virus strains, and most traits varied substantially within host range groups. Given this broad diversity, we tested for associations with growth and for signals of trade-offs between traits. Growth rate, which also varied by an order of magnitude across strains, was best explained by specific infectivity. Growth rate and specific infectivity were negatively correlated with survival in the largest host range group, which could reflect a survival-reproduction trade-off. Finally, we discovered biphasic or 'tailing' decay in all the chlorovirus groups. The nature and diversity of these traits have major implications for the ecology and evolutionary potential of the chloroviruses, and reinforce the importance of studying viral life histories.

**Keywords**

life cycle, phenotypic diversity, trade-offs, phycodnavirus, chlorovirus, *Chlorella*, flow virometry, one-step growth assay, persistence assay, non-linear models

## Introduction

Life histories play an important role in the ecology and evolution of viruses, including the vast number of microbial viruses on the planet. Viral life histories encompass 'performance' traits that influence fitness, including adsorption rate, lysogeny probability, progeny number, and mortality rate (performance sensu DeLong et al. 2022). Different traits are favored under different conditions (Abedon et al. 2003, Dessau et al. 2012, Heineman and Brown 2012, Berngruber et al. 2013), so that virus populations with diverse life histories are better able to respond to selection. Conversely, trade-offs between life history traits are likely to act as evolutionary constraints (Goldhill and Turner 2014, Keen 2014). For microbial viruses, functional constraints have been found between lysis time and burst size, for example (Abedon et al. 2003, Wang 2006), as well as growth and extracellular survival (De Paepe and Taddei 2006, Dessau et al. 2012, Heineman and Brown 2012). Life history traits also determine viral population dynamics and their effect on host mortality (Weitz 2016), which can scale up to impact entire microbial ecosystems (Suttle 2007, Record et al. 2016, Horas et al. 2018).

Despite the importance of life history traits for microbial viruses, little is known about their natural diversity (Ceyssens et al. 2011, DeLong et al. 2022). Isolating and phenotyping large numbers of viruses is labor-intensive, and viruses isolated on the same host may not be closely related. Thus studies that analyze multiple (> 3) microbial viruses typically investigate the life history diversity within a given host species (e.g. Baudoux and Brussaard 2005, De Paepe and Taddei 2006, Stenholm et al. 2008, Frois-Moniz 2014, Kahn Mirzaei and Nilsson 2015, Zago et al. 2015, Litt and Jaroni 2017) or viral ecotype (e.g. Kukkaro and Bamford 2009, Mojica and Brussaard 2014, Jurczak-Kurek et al. 2016, Zaburlin et al. 2017, Edwards and Steward 2018), rather than within a virus clade (though see Ceyssens et al. 2011). The lack of information on intraspecific phenotypic diversity makes it difficult to parameterize epidemiological models and predict evolutionary responses, and is particularly striking when contrasted with our growing understanding of viral genetic diversity (DeLong et al. 2022).

To bridge this gap, we studied a clade of phytoplankton viruses with a large number of isolated strains. Chloroviruses (family *Phycodnaviridae*, genus *Chlorovirus*) are large dsDNA viruses that infect unicellular 'chlorella-like' green algae (Van Etten et al. 2020). They have a lytic life cycle (Fig. 1). Upon adsorption, the virus digests a hole in the host cell wall through which the host' plasma membrane and virion internal membrane fuse (Thiel et al. 2010, Milrot et al. 2017, Agarkova et al. 2021). Virion-associated proteins then depolarize the host's plasma membrane, allowing viral DNA and proteins to enter (Thiel et al. 2010, Milrot et al. 2017) and preventing infection by other chloroviruses

(mutual exclusion, Greiner et al. 2009). Viral DNA is replicated in or near the nucleus, packaged into capsids in the cytoplasm, and eventually mature virions escape by lysis (Meints et al. 1986). Virions are large (~190 nm, Yan et al. 2000, Quispe et al. 2017) and have environmentally dependent decay (Van Etten et al. 1983, Agarkova et al. 2014). The chloroviruses are known to vary in genome content and plaque size (Van Etten et al. 1988, Rodrigues et al. 2022), but the life history traits have almost exclusively been measured in the type strain PBCV-1 (exceptions: Van Etten et al. 1988, Greiner et al. 2009, Quispe et al. 2017, Schiano di Visconte et al. 2022).

Our principal aim was to characterize the life history diversity of the chloroviruses. To this end, we developed efficient methods to quantify the full life cycle (adsorption, host depolarization, completion with lysis time and burst size, mortality; Fig. 1). Applying these methods to 35 chlorovirus strains revealed a high degree of trait diversity. Subsequently, we used this diversity to explore the ecological and evolutionary impact of the traits: we investigated the traits' contribution to viral population growth, and tested for signals of trade-offs between traits. This is the most thorough exploration of chlorovirus life histories to date, and provides rare insights into the diversity of phytoplankton viruses.

## Methods

We measured the life history traits of 35 chlorovirus strains using modified one-step growth and persistence assays. The modified assays are higher throughput and allow quantification of the entire life cycle (Fig. 1); they rely on the distinction between virions and infectious virions. In what follows, viruses are described as 'virions', 'depolarizing-capable virions', or 'infectious virions', and we use the terms 'multiplicity of particles (MOP)', 'multiplicity of adsorption (MOA)', and 'multiplicity of infection (MOI)'. These terms are defined for our purposes in Table 1.

### *Viruses, algae, and experimental conditions*

The genus *Chlorovirus* is divided into four groups, which are defined by their host range and share a high degree of protein sequence similarity (≥ 92.6 %, Jeanniard et al. 2013, see also Rodrigues et al. 2022). We treat the group level as corresponding to the species level, within which evolution can occur (though the NC64A viruses are paraphyletic, see below). We used viruses from three host range groups: NC64A viruses, which infect the ciliate endosymbionts *Chlorella variabilis* NC64A and *C. variabilis* Syngen 2-3; Only Syngen viruses (Osy viruses), which replicate in *C. variabilis* Syngen 2-3 but not in *C. variabilis* NC64A; and SAG viruses, which infect the heliozoon endosymbiont *Chlorella heliozoae* SAG 3.83. All of the described procedures took place in the type hosts (e.g. the NC64A viruses were amplified and assayed in *C. variabilis* NC64A).

The algal strains NC64A, Syngen 2-3, and SAG 3.83 were stored on agar slants at 4°C and inoculated into liquid medium before use. We used a modified version of BBM (Nichols and Bold 1965), with ammonium chloride substituted for sodium nitrate as a nitrogen source and double the concentration of trace element solution 4 (first used by Frickel et al. 2016). We keep the abbreviation BBM in order to distinguish our medium from the enriched "MBBM" typically used in this model system (e.g. Van Etten et al. 1983). Growth was on a shaker under the standard conditions (see below). Algae used in the assays were in late exponential phase (~$2 \times 10^6$ algae/ml in this medium).

We phenotyped 20 NC64A viruses, 7 Osy viruses, and 8 SAG viruses (Table 2). These strains were isolated from natural ponds or streams around the world between 1981 and 2017, and have been maintained as part of a stock collection since then. Lysates were stored at 4°C. Before starting the assays, we refreshed and amplified the virus stocks: 0.5 ml of the original lysate was inoculated into 10 ml of $2 \times 10^6$ algae/ml solution, left on a shaker under the standard conditions (see below) until the algae lysed (24 h or 48 h), and filtered through 0.2 µm. The resulting filtrates were stored at 4°C and their virion concentration was measured by flow cytometry (see below). The filtrates with insufficient virion concentrations were given one more round of this amplification treatment.

Algal growth and virus replication took place under the “standard conditions”, which were 20°C and constant light. Unless otherwise specified, “shaker” refers to an orbital shaker with diameter 10 mm and frequency 120 rpm. “Culture plates” are always 96-well flat-bottomed tissue culture plates (Techno Plastic Products, CH); “deep well plates” are always 96-well 2.2 ml polypropylene deep well plates (VWR International, USA). Any 4°C storage was also in the dark.

*Virion quantification with flow cytometry*

To quantify virions, we used a flow cytometry protocol based on Brussaard (2004) and Wen et al. (Wen et al. 2004). The protocol does not require fixation and can handle up to 96 samples at a time with 97-99 % repeatability (data not shown). Briefly, virus samples were mixed with SYBR Green I stain (Merck, Germany) and Tris-EDTA buffer in a PCR plate, to a final volume of 150 µl and a final SYBR Green concentration of 0.5 X. Depending on the expected virion concentration, 7.5 or 30 µl of virus sample was used. The samples were heated to 80°C for 10 min, allowed to cool for 15 min, and stained particles were counted by a flow cytometer with automated loader (BD FACSVerse, BD Biosciences, USA). Each sample was run for 30 s (40-50 µl), and the virion population was identified based on its side scatter and green fluorescence. A detailed protocol is available on protocols.io (Lievens 2022a).

*Modified one-step growth (mOSG) assay*

One-step growth assays measure the growth traits of lytic viruses by tracking a single infection cycle (Fig. 2) (Delbrück 1945, Van Etten et al. 1983, Hyman and Abedon 2009). Classically, a specific MOI of viruses is added to a host culture and given a short time to adsorb. Infections are then synchronized, for example by diluting the culture to prevent further adsorption. Solutions are sampled at regular intervals, and the accumulation of viruses is used to calculate the lysis time, burst size, and sometimes adsorption rate. We modified this assay by inoculating based on MOP, which we varied across replicates (Fig. 2) (cf. Brown and Bidle 2014, Taylor et al. 2018). By combining this modification with a statistical model of the viral life cycle, we were able to estimate the depolarization probability in addition to the adsorption rate, lysis time, and burst size. The modeling approach also enabled robust error estimation.

The modified one-step growth (mOSG) assay was performed as follows. We combined algae and viruses in culture plates; each well contained 0.1 ml solution with $1.5 \times 10^7$ algae/ml and either MOP 0.5, 1, 2, 5, or 10 of a given virus filtrate (MOP 20 was included for a few strains). The virus volumes were pipetted separately, so that the different MOPs were statistically independent. Immediately after combining algae and viruses, the solutions were mixed for 15 min to induce adsorption (1200 rpm on a microplate shaker with orbital diameter 1 mm). The infections were then synchronized by 1,000-fold dilution into nine sets of deep well plates (2 µl solution + 1998 µl BBM). The deep well plates were sealed with transparent foil and left under the standard conditions; they were inverted every hour to prevent sedimentation. At time points 0, 2, 4, …, and 16 h after dilution, we sampled a set of deep well plates: deep well plates were centrifuged for 15 min at 2000 g to separate virions from algae, after which supernatants (containing free virions) were transferred into culture plates and stored at 4°C. The independent collections maximized the statistical independence of the data. At the time of dilution, we also prepared one deep well plate containing a 1 : 10,000 dilution. It was sampled after 16 h, and served to detect signals of secondary infection (see Supp. Fig. S1M). The virion concentration in the supernatants was quantified by flow cytometry within one week of sampling. The protocol is represented schematically for one virus strain in Supp. Fig. S2; a detailed protocol is available on protocols.io (Lievens 2022b).

Next, we wrote a model to describe the concentration of free virions over the course of the mOSG assay. Free virions included the virions that had not adsorbed during the adsorption period, and the progeny virions that accumulated as infected cells lysed:

$$V(t) = \frac{1}{\delta} * \left( \underbrace{A_a * M * e^{-k*A_a*t_a}}_{\textit{unadsorbed virions}} + \underbrace{A_a * \left(1 - e^{-d*\left(1-e^{-k*A_a*t_a}\right)*M}\right) * F\left(t; \mu_l, \sigma_l^2, \alpha\right) * b_d}_{\textit{release of progeny virions}} \right) \qquad \text{(Eq. 1).}$$

Here *V(t)* is the free virion concentration at *t* hours after dilution, *M* is the MOP (0.5-20), and $\delta$ is the dilution factor (1000). To model the concentration of unadsorbed virions, we assumed that virions adsorbed at a constant rate, that all virions were capable of adsorbing, and that there were enough binding sites available for all virions (Meints et al. 1988). In this case, the concentration of unadsorbed virions at the end of the adsorption period follows a simple exponential model with adsorption constant *k*, algal concentration during the adsorption period $A_a$ ($1.5 \times 10^7$ algae/ml), duration of the adsorption period in minutes $t_a$ (15 min), and initial virion concentration $A_a*M$ (Hyman and Abedon 2009, Eq. 18.2). We assume that these virions stayed unadsorbed after dilution, i.e. that their concentration remained constant over time. To model the concentration of progeny virions, we used the findings that depolarization is necessary for chlorovirus infection (Thiel et al. 2010, Milrot et al. 2017) and prevents infection by other chloroviruses (Greiner et al. 2009). The accumulation of progeny virions over time thus depends on the concentration of depolarized cells, the time at which they lyse, and their burst size upon lysis. For the concentration of depolarized cells, we assumed that adsorbed virions were randomly distributed across host cells, and that depolarizing-capable and depolarizing-incapable virions adsorbed at the same rate. The concentration of depolarized cells at the end of the adsorption period is then derived from the Poisson distribution with expected number of events $d * \left(1 - e^{-k*A_a*t_a}\right) * M$, which is the probability that a given virion is depolarizing-capable *d* multiplied by the MOA. Next, we assumed that MOP had no effect on the average number of progeny virions produced per depolarized cell $b_d$. This crucial assumption was based on the property of mutual exclusion (all depolarized cells are infected by max. one virion, Greiner et al. 2009), and was supported by single-cell burst size data for a related chlorovirus (Lievens et al. 2022). Finally, under the simplification that all depolarized host cells produced $b_d$ virions, the distribution of lysis time could be approximated by a truncated normal distribution (in reality the burst size probably varied across cells (Delbrück 1945, Timm and Yin 2012, Lievens et al. 2022), but without single-cell information we cannot take this into account). The proportion of lysed cells over time *F(t)* is the cumulative distribution function of lysis time, with mean lysis time $\mu_l$, standard deviation $\sigma_l$, and the earliest possible lysis time α. We set α to 0 for simplicity (for the majority of the virus strains, including α as a separate parameter did not affect the fit, Supp. Fig. S3). Eq. 1 is derived in more detail in Supp. Method S1, and the parameters are summarized in Table 3. We investigated the model's sensitivity by varying each parameter and evaluating its effect on a simulated dataset; the effects are presented graphically in Supp. Fig. S4.

For each viral strain, we fit Eq. 1 to our virion concentration data using nonlinear least squares fitting ('nls' in base R version 3.6.1, R Core Team 2014). Function *F(t)* was calculated with the 'EnvStats' package (Millard 2013). The data was *ln*-transformed and curated before fitting: obvious outliers

were removed (virion concentration implausibly high or low compared to the data for other MOPs at the same time point, or compared to other time points of that MOP), as were time points with secondary infections (aberrant 1 : 1,000 vs. 1 : 10,000 dilutions data at time point 16 h, or secondary increases at later time points for low MOPs). For the fitting, all parameters were given appropriate lower limits (0 for $k$ and $d$; 0.5 for $\sigma_l$; 1 for $\mu_l$ and $b_d$). $k$, $\sigma_l$, $\mu_l$, and $b_d$ were given unrealistically high upper limits; $d$ was given a meaningful upper limit of 1. To ensure the parameter estimates were robust, we used a variety of initial parameters for each model (example in Supp. Fig. S1, panels A-D). The quality of the model fit was assessed by visually judging the fit and distribution of residuals (example in Supp. Fig. S1, panels I-O). Non-parametric bootstrapping was used to obtain 95 % CIs for each parameter (package 'nlstools', Baty et al. 2015) (example in Supp. Fig. S1, panels E-H). We also used the bootstrapped fits to look for compensating effects between the parameters (e.g. inherently correlated fits of the intercept, driven by $k$, and amplitude, driven by $b_d$) and evaluate their extent (Supp. Fig. S5). Finally, we confirmed the model's fidelity by comparing our estimates of $k$, $\mu_l$, and $b_d$ with classical calculations based on the curated virion concentration data; the two methods were highly consistent (Supp. Fig. S6).

We tested the repeatability of the mOSG assay and model in separate experiments with four MOPs (0.5, 1, 5, 10) and time points up to 14 h (results shown in Supp. Fig. S7). The repeatabilities of the point estimates were 0.86 for $k$, 0.82 for $d$, 0.51 for $\mu_l$, 0.44 for $\sigma_l$, and 0.65 for $b_d$ (n = 10, 17, 8, 8, and 16 strains, respectively, each strain tested twice; calculated following Nakagawa and Schielzeth 2010). When an effect of the testing day was included to account for environmental variation, repeatability increased to 0.76 for $\mu_l$, 0.57 for $\sigma_l$, and 0.83 for $b_d$. Note that we used more MOPs, more time points, and a single testing day in this mOSG assay, so our power was certainly higher.

*Modified persistence (mP) assay*

Persistence assays (also: survival, inactivation, or decay assays) measure a virus' environmental mortality by tracking the decline in infectious viruses over time. Typically, the concentration of infectious viruses at each time point is estimated via serial dilution methods (e.g. plaque or most probable number assays), and the mortality rate is calculated from these estimates (Fig. 3, Suttle and Chan 1994, De Paepe and Taddei 2006). We modified this assay by using initial virus solutions with known virion concentrations, which allowed the estimation of the specific infectivity in addition to the mortality rate (Fig. 3). The data also supported the existence of an additional trait, the robust fraction (see below and Fig. 1). We used a statistical model to estimate these traits from the raw data, which maximized the power per data point and avoided compounding errors from per-time-point calculations.

The modified persistence (mP) assay was run as follows. First, we produced "fresh" viruses by amplifying viruses in 10 ml of $1 \times 10^6$ algae/ml solution. The amplification was started with a modest number of virions (~$5 \times 10^5$ virions/ml) and incubated for 24 h on a shaker under the standard conditions. After 24 h, solutions were filtered through 0.45 µm, and the virion concentrations in the filtrates were immediately quantified by flow cytometry. We then prepared virion solutions with different concentrations: in deep well plates, we combined filtrates and BBM to produce 1.5 ml solutions containing $5 \times 10^4$, $5 \times 10^3$, $5 \times 10^2$, and $5 \times 10^1$ virions/ml of a given virus strain. The filtrate volumes were pipetted separately, so that the different dilutions were statistically independent. The solutions were mixed and aliquoted into five sets of culture plates, which were sealed with transparent foil and left under the standard conditions. After 0, 7, 14, 21, and 28 days, we used a set of culture plates to measure the concentration of infectious virions in each solution: 10 µl from each solution was added to 16 culture wells containing 190 µl of $1.05 \times 10^6$ algae/ml solution (also in culture plates). These were kept on a shaker under the standard conditions for 4 days, after which we measured the $OD_{680}$ to determine which culture wells contained viable algae (virus-negative) and which did not (virus-positive). Using aliquots instead of longitudinal sampling maximized the statistical independence of the data. The protocol is represented schematically for one virus strain in Supp. Fig. S2; a detailed protocol is available on protocols.io (Lievens 2022c).

Over time, the proportion of virus-positive wells decreased. We modeled this decline as

$$P(t) = 1 - e^{-(V*s*r+V*s*(1-r)*e^{-m*t})} \quad \text{(Eq. 2).}$$

This is a biphasic decay model, which assumes that infectious virions can be either "fragile", i.e. susceptible to decay, or "robust", i.e. immortal. We used this model because the exponential decay model was a poor fit for many of our virus strains (Supp. Fig. S8, Supp. Method S1). This biphasic parametrization was the simplest extension of the exponential model, and fit our data very well. In the model, *P(t)* is the proportion of virus-positive wells after *t* days under the standard conditions, and $V * s * r + V * s * (1 - r) * e^{-m*t}$ is the expected number of infectious virions added to each culture well. *V* is the initial number of virions (e.g. 10 µl of a $5 \times 10^4$ virions/ml solution = 500 virions), *s* is the frequency of infectious virions when the solution is fresh (the specific infectivity), and *r* is the fraction of those virions that is robust. The fragile infectious virions (fraction 1-*r*) decay exponentially with mortality rate *m*. The probability that at least one infectious virion was added to a well is derived from the Poisson distribution. Eq. 2 is derived in more detail in Supp. Method S1, and the parameters are summarized in Table 3. We investigated the model's sensitivity by varying each parameter and evaluating its effect on a simulated dataset; the effects are presented graphically in Supp. Fig. S9.

For each viral strain, we fit Eq. 2 to the data using generalized nonlinear regression models, with the number of virus-positive and -negative wells as a binomial response variable (in R version 3.6.1, R Core Team 2014, package 'gnlm', Swihart and Lindsey 2019). The parameters *s*, *r*, and *m* were inverse logit-transformed to keep them in the interval [0,1] (*m* can be larger than 1, but in practice the mortality rates were much lower). To ensure the parameter estimates were robust, we used a variety of initial parameters for each model (example in Supp. Fig. S10, panels A-C). The quality of the model fit was assessed by visually judging the fit and distribution of residuals (example in Supp. Fig. S10, panels G-L). Parametric bootstrapping was used to obtain 95 % CIs for each parameter (example in Supp. Fig. S10, panels D-F). We also used the bootstrapped fits to look for compensating effects between the parameters (e.g. inherently correlated fits of the intercept *s* and slope *m*) and evaluate their extent (Supp. Fig. S5). Finally, we confirmed the model's fidelity by comparing our estimates of *s, m*, and *r* with classical calculations based on the most probable number of infectious virions at each time point; the two methods were highly consistent (Supp. Fig. S6).

We tested the repeatability of the mP assay and model in a separate experiment, which confirmed the biphasic decay pattern and the consistency of the fits for *s*, *r*, and *m* (results shown in Supp. Fig. S11).

*Comparison of mOSG and mP assays*

By comparing the results of the mOSG and mP assays, we could derive the final traits in the life cycle: the probability that a depolarized cell completes the life cycle (*c*) and the burst size per completed cell ($b_c$) (Fig. 1). We define "completion" as lysis with release of virions. The completion probability *c* could be derived from the specific infectivity *s* and the depolarization probability *d* (see Fig. 1):

$$c = s/d \qquad \text{(Eq. 3).}$$

We could then derive the average burst size per completed cell $b_c$ as

$$b_c = b_d/c \qquad \text{(Eq. 4),}$$

because the burst size of depolarized cells that don't complete the life cycle is 0 (see Fig. 1). The bootstraps from the mOSG and mP assays were used to calculate confidence intervals for *c* and $b_c$.

Eq. 3 combines estimates from two experiments, and should thus be approached with caution. One difference was that the filtrates used for the mOSG assay were stored at 4°C for 2-8 days before the assay, and the mP assay filtrates were not. However, previous experiments showed that *s* is unaffected by 4°C storage for at least 9 days (J. Clot & E.J.P. Lievens, unpublished data for strain PBCV-1), so this difference was unlikely to affect our calculations. A second difference was that the algae were centrifuged before the mOSG experiment to concentrate them. This may have affected the algae's susceptibility to depolarization (i.e. *d*) or stability when infected (i.e. *c*), although previous

experiments did not support an effect of centrifugation on *s* (i.e. on *d*c*; E.J.P. Lievens & M. Spagnuolo, unpublished data for strain PBCV-1). If the algae were changed by centrifugation, we would expect the strains in each virus group to be affected equally. Finally, due to Covid-19 restrictions there was a 3-month delay between the two experiments, and we had to use separate batches of the host algae. The batches were grown from the same agar slants, however, so at most we could expect an environmental effect on *s* that affected all strains within a group. Independent evidence supporting the comparability of the mOSG and mP assays comes from single-cell burst size data for a virus related to PBCV-1 (PBCV-1-RK-M2, Lievens et al. 2022), which measured a similar burst size per completed infection $b_c$ as estimated here for PBCV-1 (~1800 and ~1400 virions, respectively).

*Growth assay*

Finally, we used the "fresh" filtrates prepared at the start of the mP assay to measure viral growth. For each viral strain, fresh filtrate was combined with the appropriate alga in a culture plate (2 wells per strain), to a final volume of 0.2 ml containing $1 \times 10^6$ algae/ml and 2,500 or 25,000 virions/ml. The solutions were incubated on a shaker under the standard conditions for 24 h, and then centrifuged for 15 min at 2000 g to separate algae and viruses. The virion concentration of the supernatants was measured by flow cytometry; the relative increase in virion concentration was used as the measure of viral growth ("relative growth"; mean of 2 replicates). For the statistical analyses, we calculated the "observed growth rate" as the natural logarithm of the relative growth divided by 24 h.

*Statistical analysis of the trait results*

Our statistical analyses explored the diversity of the traits, investigated their relationship with growth, and looked for potential trade-offs. The analyses excluded trait estimates from incomplete assays ($d$, $\mu_l$, $\sigma_l$, $b_d$, $c$, and $b_c$ for strains that did not finish growing in the mOSG assay; $r$ and $m$ for strains that did not decay in the mP assay), estimates derived from poorly fitting models, and estimates with uninformatively broad CIs compared to the plausible phenotypic range (criteria: CI > 0.67 for $d$, $s$, and $c$; CI spanning more than an order of magnitude for $b_d$, $r$, and $b_c$; CI overlapping with the upper fitting constraint for $k$, $\mu_l$, $\sigma_l$, and $m$). Details on exclusion are provided in Supp. Table S1, and estimates excluded due to poor or imprecise model fits are marked in red in Fig. 4. All analyses were performed in R version 3.6.1 (R Core Team 2014).

First, we partitioned the chlorovirus' phenotypic diversity within and among virus groups (NC64A, SAG, and Osy viruses). We fit ANOVAs to test for a group effect on each trait, with traits $b_d$, $b_c$, and $r$

*ln*-transformed to normalize their distributions. Holm's method was used to correct for multiple testing (Holm 1979). Note that these ANOVAs are not intended to distinguish between the effects of group and relatedness (phylogenetic dependence, Garland et al. 1993).

Second, we examined the relationship between the virus' life history traits and their growth. First, the observed growth rate was compared with a growth rate predicted from the mOSG and mP traits. The predicted growth rate was calculated as De Paepe & Taddei's multiplication rate ($s * b_c * \mu_l^{-1}$)(2006) with an additional adsorption term: $(1 - e^{-k*A_g}) * s * b_c * \mu_l^{-1}$ or equivalently $(1 - e^{-k*A_g}) * d * b_d * \mu_l^{-1}$. Here $A_g$ is the algal concentration during the growth assay, i.e. $1 \times 10^6$ algae/ml. The two measures were compared using Spearman's rank correlation. Second, we used generalized additive regression models to identify the life history traits that best explained the variation in observed growth rate (package 'mgcv', Wood 2017). The point estimates of the traits that could be expected to drive the first 24 h of viral growth were used as predictor variables; these were $s$, $k$, $\mu_l$, $b_c$ (*ln*-transformed), and genome size. Smooths were used when the data suggested a non-linear relationship. All possible predictor combinations were compared using the corrected Akaike Information Criterion (AICc, Akaike 1974); traits that appeared in every regression model with a difference of ≤ 2 ΔAICcs compared to the best model were considered to be well-supported (Burnham and Anderson 2004).

Third, we used correlational analyses to look for signals of trade-offs that are commonly found or suggested in the literature (listed in Table 4). This analysis focused on the NC64A viruses, as they were assayed in the same algal strain. The hypothesized correlations were tested using Spearman's rank correlations, weighted by the precision of each estimate (1/√(product of the CI breadth of trait 1 and trait 2, package 'weights', Pasek 2021). Holm's method was used to correct for multiple testing (Holm 1979). As trade-offs can be masked by quality effects in correlational analyses (Stearns 1989), we repeated this analysis for the subset of "highest quality", i.e. fastest-growing, NC64A viruses.

**Results**

We analyzed the life history diversity within and across chlorovirus groups, the relationship between traits and growth rate, and the potential for life history trade-offs. We considered only the 'retained' trait estimates in these analyses (black in Fig. 4, listed in Supp. Table S1). There were compensating effects in the mOSG and mP model fitting (between traits $d$ & $b_d$, $\mu_l$ & $\sigma_l$, $\mu_l$ & $b_d$, $\sigma_l$ & $b_d$, $s$ & $m$, and $s$ & $r$; Supp. Fig. S5), but they were small compared to the scale of phenotypic variation (Supp. Fig.

S12). Thus the compensating effects did not prevent useful distinctions between the trait estimates. The exceptions were *s* & *m* and *s* & *r* in the subset of viral strains with $s > 0.05$, where the scale of phenotypic variation was reduced (Supp. Fig. S12C&F).

The virus traits were remarkably diverse, with trait estimates varying by a factor of 5 to 75 between strains (Fig. 4). Chlorovirus group explained a significant proportion of the variance for the adsorption constant $k$, mean lysis time $\mu_l$, SD of lysis time $\sigma_l$, and burst size per depolarized cell $b_d$ (proportions respectively 0.33, 0.86, 0.69, 0.57; $p$ respectively 0.01, < 0.0001, < 0.0001, < 0.01; Supp. Table S2). The groups had overlapping trait ranges for all traits except mean lysis time $\mu_l$ (Fig. 4, lower panels).

The virus' relative growth ranged from 1.05- to 24,628-fold increases in virion concentration in 24 h (Fig. 5A), corresponding to an observed growth rate of 0.002-0.42. The observed growth rate was correlated with the predicted growth rate ($\rho = 0.51$, $p = 0.02$; Fig. 5B), despite a small group of outliers (four NC64A strains with higher growth than predicted, top left in Fig. 5B). To identify the life history traits that best explained the variation in observed growth rate, we regressed it onto the traits that are likely to affect short-term growth: adsorption constant $k$, specific infectivity $s$, mean lysis time $\mu_l$, burst size per completed cell $b_c$, and genome size. As $\mu_l$ and $b_c$ were unresolved for several strains, we constructed two regression models: a model with predictors $s$, $k$, and genome size ($n = 30$ strains, open and solid points in Fig. 5C), and a model with predictors $s$, $k$, $\mu_l$, $b_c$, and genome size ($n = 20$ strains, solid points in Fig. 5C). In the first regression model, specific infectivity $s$ had a saturating positive effect on the observed growth rate (dashed line in Fig. 5C; $\Delta$AICc ≥ 22.6, Supp. Table S3). In the second regression model, there was ambivalent support for a linear positive effect of specific infectivity $s$ and a saturating positive effect of mean lysis time $\mu_l$ (both appeared in two out of three models with a difference of ≤ 2 $\Delta$AICcs; Supp. Table S3).

We used our largest virus group, the NC64A viruses, to look for evidence of life history trade-offs (Table 4). Short-term virion quality, represented by the specific infectivity $s$, was significantly correlated with long-term virion quality in the form of mortality rate $m$ ($\rho = 0.83$, $p = 0.0003$; Fig. 6 and Supp. Fig. S13, Supp. Table S4). The mortality rate $m$ was also correlated with the observed growth rate ($\rho = 0.76$, $p = 0.002$; Fig. 6 and Supp. Fig. S13, Supp. Table S4). The other hypothesized correlations were not significant (Fig. 6, Supp. Table S4). Because overall quality can confound the detection of constraints (Stearns 1989), we repeated the analysis on the 12 fastest-growing NC64A viruses (AN69C, CA-4A, CV-K1, CvsA1, IL-3A, IL-5-2s1, MA-1E, NE-JV-4, NYs-1, PBCV-1, WNE-10B-L2, and XZ-4A; Fig. 5A, Supp. Table S1). As all the fastest-growing strains had specific infectivity $s > 0.05$,

we did not consider the correlations between *s* and mortality rate *m* or robust fraction *r* (see above & Supp. Fig. S12C&F). None of the tested correlations were significant in this subset (Supp. Table S4).

**Discussion**

Life histories shape the epidemiology, ecosystem effects, and evolutionary potential of microbial viruses, but are rarely measured within a clade. In this study, we modified classical methods to quantify the life history traits of 35 chloroviruses from the NC64A, Osy, and SAG host range groups. We found high trait diversity within and between groups, and used this diversity to identify traits associated with growth and potential life history trade-offs. We discuss these findings, and highlight new insights into the chlorovirus life cycle, below.

*High trait diversity within and across chlorovirus groups*

The first goal of our study was to explore the trait diversity of the chloroviruses, which could be expected to influence their evolvability and the range of their ecological effects. Our results show that the chloroviruses vary substantially in every life history trait, both within and between virus groups (Fig. 4). The virion and virocell traits we measured were likely mediated by interactions between the viral genotype, the host genotype, and the environment ($G_V$ x $G_H$ x E interactions), which should be considered when comparing traits between groups and with other studies.

We can assume that the within-group diversity in chlorovirus traits is a consequence of genetic variation, as the strains were tested in the same host and environment ($G_H$ and E kept constant). This genetic association would enable an evolutionary response if selection favors a particular phenotype, which may happen during the course of an epidemic (Frank 1996, Bolker et al. 2010, Berngruber et al. 2013), as host densities change (Abedon et al. 2003, Heineman and Bull 2007), or in response to abiotic changes (Alizon et al. 2009, Dessau et al. 2012, Heineman and Brown 2012). The occurrence of chlorovirus evolution in nature is supported by work on NC64A, Osy, and SAG viruses in natural ponds (Quispe et al. 2016), which showed that the frequencies of plaque size phenotypes varied over the course of a year. Combining trait data with genomic data (e.g. Jeanniard et al. 2013, Rodrigues et al. 2022) could allow the construction of a genotype-to-phenotype map to further explore chlorovirus evolution (DeLong et al. 2022).

Attributing the between-group variation to genetic differences is more difficult, as the viruses were not tested on a common host (only E kept constant). It is intriguing, however, that the SAG viruses had shorter lysis times and slower adsorption. The SAG viruses infect *C. heliozoae*, which forms endosymbioses with the heliozoan *Acanthocystis turfacea*, while the NC64A and Osy viruses infect *C.*

*variabilis*, which symbioses with the ciliate *Paramecium bursaria* (Van Etten et al. 2020). Predation of *P. bursaria* is known to affect the growth of chlorovirus Osy-NE-ZA1 (DeLong et al. 2016, 2018, Al-Ameeli et al. 2021), and it is possible that chlorovirus traits respond to the broader ecological context of the heliozoan or ciliate hosts.

The natural phenotypic diversity is likely to be even higher than the 5- to 75-fold range we measured. Previous work has shown that the expression of chlorovirus traits depends on the host genotype ($G_H$ effects, Quispe et al. 2017) and on environmental (E) effects such as light conditions (Van Etten et al. 1983, I.V. Agarkova unpublished data), temperature (Horas et al. 2018, I.V. Agarkova unpublished data), nutrient ratios (Clasen and Elser 2007, Cheng et al. 2015), and the host's growth phase (Van Etten et al. 1983, E.J.P. Lievens unpublished data). It is likely that these effects interact with virus strain ($G_V$ x $G_H$ and $G_V$ x E effects) and with each other ($G_H$ x E and $G_V$ x $G_H$ x E effects), further enriching the overall phenotypic diversity. Interestingly, the relative lysis times we found corresponded well to previous studies of multiple chloroviruses, but the relative burst sizes did not (Supp. Table S1, Van Etten et al. 1988, Schiano di Visconte et al. 2022). This suggests that different traits have different $G_V$ x E effects, as found in other host-parasite systems (Hall et al. 2017). Future research could examine the extent and functional basis of this (lack of) plasticity.

*Specific infectivity best explains growth rate*

We used complementary bottom-up and top-down approaches to investigate chloroviral growth. First, extrapolating the virus' growth from their life history traits produced meaningful predictions of the variation in observed growth rate (bottom-up, Fig. 5B) (De Paepe and Taddei 2006, Weitz 2016, Edwards et al. 2021). However, the top-down approach found that specific infectivity was the only trait to explain this variation, and that only in the unrestricted dataset (dashed line in Fig. 5C). In the restricted dataset, which included information on lysis time and burst size, none of the traits had detectable effects on the observed growth rate. The lack of top-down signals in the restricted dataset was probably due to saturation in the growth assay: if the faster-growing strains lysed all of the host cells, the variation in growth would be artificially reduced and effects of e.g. lysis time could be obscured. This explanation is supported by the saturating effect of *s* in the unrestricted dataset (dashed line in Fig. 5C): if growth had been uninhibited, we would expect a linear effect. In the future, growth assays with shorter durations or smaller inocula could be useful to analyze the traits that most contribute to chlorovirus growth.

One cluster of NC64A strains grew much more than predicted: AN69C, CvsA1, IL-3A, and WNE-10B-L2 (top left in Fig. 5B). Interestingly, these four strains had the lowest burst sizes of the NC64A viruses ($b_d$, Supp. Table S1). The strains may have been particularly sensitive to the differences between the

mOSG and growth assays (e.g. shaking frequency, algal batch), for example through reduced burst size. An alternative possibility is that an unmeasured trait had a strong influence on the growth of these strains (e.g. extracellular matrix production, Graves et al. 1999, Kawasaki et al. 2002).

*Negative correlation between survival and growth in the NC64A viruses*

We used our largest virus group, the NC64A viruses, to look for trait correlations that could suggest the existence of trade-offs among life history traits. While correlations cannot prove or disprove that a functional constraint exists (Stearns 1989, Zera and Harshman 2001, Agrawal et al. 2010), they are an important explorative step and allow comparisons with the existing literature.

We found that viruses with higher mortality rates had higher observed growth rates and specific infectivities (Fig. 6). Given that the observed growth rate mostly depended on the specific infectivity (Fig. 5C), this pattern can best be described as a negative correlation between survival and growth. The pattern was driven by the slowest-growing strains, which all belonged to the NY-2A clade (AR158, MA-1D, NY-2A, NY-2B, Supp. Table S1). This finding could reflect a trade-off between survival and reproduction, as found in phages (Table 4; correlations: De Paepe and Taddei 2006, Dessau et al. 2012, confirmed trade-offs: Heineman and Brown 2012, García-Villada and Drake 2013), with an extreme survival strategy evolving in the NY-2A clade. Alternatively, the negative correlation between long-term and short-term success could reflect an ecological difference. For example, the NY-2A clade could contain slow-growing strains because they are adapted to a different host genotype (thus performing poorly in *C. variabilis* NC64A) whose ecology favors very slow decay. Observations of the short- and long-term success of chloroviruses under more natural conditions, and in a greater range of host genotypes, would be necessary to distinguish between these possibilities.

The other hypothesized trade-offs were not supported in the NC64A viruses, and this was not explained by variation in quality. In particular, we did not find a relationship between lysis time and burst size, which has been suggested as a general trade-off for lytic viruses (Goldhill and Turner 2014). Replacing the burst size per depolarized cell $b_d$ with the burst size per completed cell ($b_c$), infectious burst size ($s*b_c$), or nucleotide production per completed cell (genome size*$b_c$) also failed to produce a correlation with $\mu_l$ (data not shown). The one-dimensional trade-off between lysis time and burst size may be obscured by other differences between the strains, or may not exist for the NC64A viruses.

*New insights into chlorovirus life cycles: failure to depolarize vs. failure to complete*

Not all depolarized cells lead to completed infections (Quispe et al. 2017). Defective virions are a well-known aspect of virus biology (Klasse 2015), and in chloroviruses they include empty capsids

and capsids with different membrane conformations (strain PBCV-1, Agarkova et al. 2014). The chlorovirus' failure rate was generally high; depending on the strain, only 0.4-24 % of freshly-produced virions were infectious (specific infectivity *s*, Fig. 4). Our estimates of *s* were lower than those found previously, e.g. 10 % compared to 25-30 % for PBCV-1 (Van Etten et al. 1983). This difference might be explained by the lower richness of the medium for the algal host (Bratbak et al. 1998, cf. Tseng and Myers 2014, Maat and Brussaard 2016, Bachy et al. 2018), by a difference in sensitivity of liquid culture vs. plaque assays, or by a higher concentration of attachment-blocking host receptors in our virus solutions (Agarkova et al. 2021). It is also possible that *s* was underestimated in our mP assay because wells inoculated with very small numbers of infectious virions did not lyse within four days (especially likely for slow-growing strains).

We were able to separate viral failure into performance traits: an inability to depolarize the host cell and an inability to complete the life cycle. The depolarization probability varied widely between strains (Fig. 4). The 'depolarization' step in our model actually includes three events: first, the host cell wall is digested by a conserved virion protein, PBCV-1 A561L-homolog (Agarkova et al. 2021); next, the viral and host membranes fuse, most likely due to turgor pressure in the host cell (Thiel et al. 2010); finally, virion-associated $K^+$ channel proteins depolarize the cell (Frohns et al. 2006, Thiel et al. 2010). The ability to successfully depolarize a host is therefore dependent on specific, pre-packaged virion proteins (it is a virion trait, DeLong et al. 2022). We hypothesize that the interstrain variation in depolarization probability is caused by variation in the efficiency or copy number of the A561L-homolog or $K^+$ channel proteins (K+ channel proteins vary across strains, Frohns et al. 2006, PBCV-1 has ~60 copies of A561L-homolog, Dunigan et al. 2012). Transcriptomic or proteomic studies on multiple virus strains should shed light on the underlying mechanism.

Surprisingly, we find that an inability to complete the life cycle is the biggest hurdle for chloroviruses. In all but one strain, fewer than half of the depolarized host cells produced progeny virions (completion probability $c$ = 0.01-0.42, Fig. 4). These low values may have been affected by an underestimate in our measurement of the specific infectivity *s* (see above), which would have led to an underestimate of $c$ (and an overestimate of $b_c$). Alternately, they may have been biased by our assumption that all virions were capable of adsorbing: if there was a 'residual fraction' $f$ of non- or slow-adsorbing virions (Gallet et al. 2012), the specific infectivity would actually be $s = (1-f)*d*c$, and we would also have underestimated $c$ (and overestimated $b_c$). Yet even if the specific infectivity was twice as high, or half of the virions were incapable of adsorbing, the corrected completion probability would fall below 50 % for most strains. Completion probability is a virocell trait that depends on both host and virus (DeLong et al. 2022). If the virus effect is the most important, then we expect the completion probability to reflect the proportion of virions with inherent faults

(Agarkova et al. 2014). Alternately, the interaction between virus and host could be most important: algal cells probably vary in competence, e.g. through variation in their physiological states (cf. Clasen and Elser 2007, Cheng et al. 2015) or expression of defense pathways (Rowe et al. 2013), and some virus strains could be more susceptible to this variation. More susceptible virus strains could be evolutionarily mismatched with the host or susceptible to trade-offs with some other virus trait (Goldhill and Turner 2014).

*New insights into chlorovirus life cycles: biphasic persistence*

We discovered that many chloroviruses have biphasic or "tailing" persistence, with 0-10 % of the initial infectious virions being resistant to decay in our experiment (robust fraction *r*, Fig. 1 & 3). Biphasic decay is found in many viruses, and can be caused by several factors. 1) Changes in medium properties through time (Hiatt 1964). In this case we would have expected the same biphasic pattern to occur across all strains, so this is not likely. 2) Adhesion to organic particles (Agarkova et al. 2014, Pinon and Vialette 2018). In this case, we would expect to see a larger robust fraction in the fast-growing strains, because they caused more lysis in the first step of the mP assay, and thus produced more organic matter. We do not see this pattern (e.g. *r* between 0.1 and 5 % for the fast-growing NC64A viruses, Fig. 4). 3) Viral aggregation (Pinon and Vialette 2018). Chloroviruses probably aggregate, and different strains could vary in their tendency to do so. 4) Two concurrent mortality processes causing differing degrees of damage (Koch 1960, Hiatt 1964, Roy et al. 1982, cf. Beck et al. 2014). If the first process (e.g. damage to the capsid) occurs rapidly but leaves some probability of successful infection, and the second process (e.g. DNA denaturation) occurs slowly and leads to complete inactivation, biphasic kinetics emerge. The variation between strains could be due to variation in the stability of the two targets of inactivation; the strains where $r = 0$ would then lack one target or have both decay at the same rate. 5) The presence of a more resistant subpopulation with slower decay. These might be virions with fewer production errors (Beauchemin et al. 2019), or virions with a specifically different phenotype (Hiatt 1964, Brouwer et al. 2017).

For possibilities 3-5, we could expect selection to optimize decay in response to each strain's native environment. Selection could act synergistically on the mortality rate *m* and robust fraction *r* to produce high vs. low-persistence types (though we don't see this pattern in the NC64A viruses, Fig. 6). Alternatively, the robust fraction could reflect an adaptation to uncertainty in the environment. If long-term persistence comes at a cost of short-term success (see above), then producing two virion types could allow chloroviruses to profit from patches of concentrated algae (Frank 1996, Berngruber et al. 2013) and to survive their seasonal environments (Long and Short 2016). In this case, biphasic persistence could be a bet-hedging strategy (constant *r*) or a plastic strategy (*r* varying in response to

environmental cues); both types have been demonstrated for various virus traits (bet-hedging: Gallet et al. 2012, Leggett et al. 2013, Erez et al. 2017, Chaturvedi et al. 2020, plasticity: Bruce et al. 2021).

It is striking that we find biphasic decay in all the chlorovirus groups, because the existing work on phytoplankton viruses typically assumes exponential decay (i.e. mortality at a constant rate; Suttle and Chan 1994, Cottrell and Suttle 1995, Garza and Suttle 1998, Šulčius et al. 2015, Long and Short 2016, Demory et al. 2017, 2021a, 2021b). Though assuming exponential decay may be appropriate in many cases, it seems unlikely that the chloroviruses are the only algal viruses with a robust fraction (e.g. possible non-linearity in Tomaru et al. 2005). Finding biphasic decay in other phytoplankton viruses could resolve some questions about their ecology, such as their ability to form "seed banks" that persist outside blooms (Long and Short 2016). It would also affect our understanding of aquatic microbial communities and nutrient cycling, in which viral infection and decay play important roles (Mojica and Brussaard 2014).

*Applicability of the methods and future work*

We hope that these methods will be useful to other virologists interested in life history traits. By leveraging the distinction between MOP and MOI, the mOSG and mP assays measure more traits than assays based on one or the other (e.g. Van Etten et al. 1983, Tomaru et al. 2005, Taylor et al. 2018). The high-throughput flow cytometry makes them more efficient than e.g. quantification through plaque assays, and the statistical modeling maximizes the information gained from each data point. The assays should be applicable to any culturable lytic virus that can be counted on a flow cytometer, which now includes many aquatic (Brussaard 2004) and human viruses (Lippé 2018). Precision could be increased by increasing the sampling resolution, including more MOPs, or replicating MOP treatments. The statistical models could also be edited to reflect life cycle differences. For example, our models assume that burst size is constant because multiple infections do not occur (discussed below). This is equivalent to a system where multiple infections occur, but do not affect burst size. If multiple infections are possible and do affect burst size, the equations could be extended to include a facilitation or competition factor. Finally, in systems where no information is available, some inferences can be made from the relative amplitudes of the mOSG curves. These should be related to MOP via a Poisson probability function if burst size is independent of MOP (Supp. Fig. S14).

Further work on the chlorovirus life cycles could support or refute some aspects of our models. As discussed above, we assumed there was no 'residual fraction' during adsorption, and that robust infectious virions never decay (Fig. 1). These are probably unrealistic assumptions, which could be tested by longer studies of adsorption or persistence. We also assumed that all mOSG parameters

were independent of MOP. Mutual exclusion prevents coinfection in chloroviruses (Greiner et al. 2009), and we assumed that established infections were unaffected by other virions attaching to or digesting the cell wall of the host. Our data was consistent with this assumption, but it had limited power to detect deviations for $d$ and $b_d$ (Supp. Fig. S14). A recent study confirmed that burst size was unaffected by MOP in a chlorovirus related to PBCV-1 (MOP 1 vs. 10, Lievens et al. 2022), but previous work did find an effect of MOI on burst size in PBCV-1 (MOI 0.1-50, Van Etten et al. 1983). It may be that these effects are restricted to very high MOPs/MOIs, when 'lysis from without' and dual infection can occur (Tessman 1985, Chase et al. 1989). Future work may need to incorporate MOP-dependencies, especially at higher MOPs (cf. Brown and Bidle 2014, Taylor et al. 2018).

**Conclusion**

A proper understanding of the ecological impact and evolutionary potential of viruses rests on a knowledge of their life history traits. We showed that the chloroviruses have high phenotypic diversity across their entire life cycle, both within and across host range groups. This suggests that they are evolutionarily flexible, although they may be constrained by a survival-reproduction trade-off. The chloroviruses also had large variation in growth and long-term persistence capabilities, which is likely to have strong effects on their ecology. These results confirm the importance of studying viral life histories, and will hopefully prompt similar research into other virus clades.

**Acknowledgements**

E.J.P.L. thanks J. Pantel, M. Hartfield, and N. Lustenhouwer for feedback on the statistical modeling and model presentation; J. Clot for help with the viruses; R. Hermann for transferring algae during lockdown; and the University of Konstanz Young Scholar Fund for material support. We acknowledge the flow cytometry centre (FlowKon) at the University of Konstanz for the use of flow cytometers and the expert support in instrument usage and data analysis. We also thank the editor and two anonymous reviewers for their constructive feedback.

**Data availability**

Data and analyses are available at doi:10.5281/zenodo.6573770.

**References**

Abedon, S. T., P. Hyman, and C. Thomas. 2003. Experimental Examination of Bacteriophage Latent-Period Evolution as a Response to Bacterial Availability. Applied and Environmental Microbiology 69:7499–7506.

Agarkova, I., B. Hertel, X. Zhang, L. Lane, A. Tchourbanov, D. D. Dunigan, G. Thiel, M. G. Rossmann, and J. L. Van Etten. 2014. Dynamic attachment of Chlorovirus PBCV-1 to *Chlorella variabilis*. Virology 466–467:95–102.

Agarkova, I. V., L. C. Lane, D. D. Dunigan, C. F. Quispe, G. A. Duncan, E. Milrot, A. Minsky, A. Esmael, J. S. Ghosh, and J. L. Van Etten. 2021. Identification of a chlorovirus pbcv-1 protein involved in degrading the host cell wall during virus infection. Viruses 13:1–19.

Agrawal, A. A., J. K. Conner, and S. Rasmann. 2010. Tradeoffs and Negative Correlations in Evolutionary Ecology. Pages 243–268 *in* M. A. Bell, W. F. Eanes, D. J. Futuyma, and J. S. Levinton, editors. Evolution After Darwin: the First 150 Years. Sinauer Associates.

Akaike, H. 1974. A new look at the statistical model identification. IEEE Transactions on Automatic Control 19:716–723.

Al-Ameeli, Z. T., M. A. Al-Sammak, J. P. DeLong, S. Thomas, D. D. Dunigan, and J. L. Van Etten. 2021. Catalysis of chlorovirus production by the foraging of *Bursaria truncatella* on *Paramecia bursaria* containing endosymbiotic algae. Microbial Ecology 9:2170.

Alizon, S., A. Hurford, N. Mideo, and M. Van Baalen. 2009. Virulence evolution and the trade-off hypothesis: history, current state of affairs and the future. Journal of Evolutionary Biology 22:245–59.

Bachy, C., C. J. Charlesworth, A. M. Chan, J. F. Finke, C. H. Wong, C. L. Wei, S. Sudek, M. L. Coleman, C. A. Suttle, and A. Z. Worden. 2018. Transcriptional responses of the marine green alga *Micromonas pusilla* and an infecting prasinovirus under different phosphate conditions. Environmental Microbiology 20:2898–2912.

Baty, F., C. Ritz, S. Charles, M. Brutsche, J. Flandrois, and D.-M. M. 2015. A Toolbox for Nonlinear Regression in R: The Package nlstools. Journal of Statistical Software 66:1–21.

Baudoux, A.-C., and C. P. D. Brussaard. 2005. Characterization of different viruses infecting the marine harmful algal bloom species *Phaeocystis globosa*. Virology 341:80–90.

Beauchemin, C. A. A., Y.-I. Kim, Q. Yu, G. Ciaramella, and J. P. DeVincenzo. 2019. Uncovering critical properties of the human respiratory syncytial virus by combining in vitro assays and in silico analyses. PLoS ONE 14:e0214708.

Beck, S. E., R. A. Rodriguez, K. G. Linden, T. M. Hargy, T. C. Larason, and H. B. Wright. 2014. Wavelength dependent UV inactivation and DNA damage of adenovirus as measured by cell culture infectivity and long range quantitative PCR. Environmental Science and Technology 48:591–598.

Belshaw, R., A. Gardner, A. Rambaut, and O. G. Pybus. 2008. Pacing a small cage: mutation and RNA viruses. Trends in Ecology and Evolution 23:188–193.

Berngruber, T. W., R. Froissart, M. Choisy, and S. Gandon. 2013. Evolution of virulence in emerging epidemics. PLOS Pathogens 9:e1003209.

Bolker, B. M., A. Nanda, and D. Shah. 2010. Transient virulence of emerging pathogens. Journal of the Royal Society Interface 7:811–822.

Bratbak, G., A. Jacobsen, M. Heldal, K. Nagasaki, and F. Thingstad. 1998. Virus production in *Phaeocystis pouchetii* and its relation to host cell growth and nutrition. Aquatic Microbial Ecology 16:1–9.

Brouwer, A. F., M. C. Eisenberg, J. V. Remais, P. A. Collender, R. Meza, and J. N. S. Eisenberg. 2017. Modeling Biphasic Environmental Decay of Pathogens and Implications for Risk Analysis. Environmental Science and Technology 51:2186–2196.

Brown, C. M., and K. D. Bidle. 2014. Attenuation of virus production at high multiplicities of infection in *Aureococcus anophagefferens*. Virology 466–467:71–81.

Bruce, J. B., S. Lion, A. Buckling, E. R. Westra, and S. Gandon. 2021. Regulation of prophage induction and lysogenization by phage communication systems. Current Biology 31:5046–5051.

Brussaard, C. P. D. 2004. Optimization of procedures for counting viruses by flow cytometry. Applied and Environmental Microbiology 70:1506–1513.

Burnham, K. P., and D. R. Anderson. 2004. Multimodel Inference: Understanding AIC and BIC in Model Selection. Sociological Methods & Research 33:261–304.

Ceyssens, P.-J., T. Glonti, A. M. Kropinski, R. Lavigne, N. Chanishvilli, L. Kulakov, N. Lashki, M. Tediashvili, and M. Merabishvili. 2011. Phenotypic and genotypic variations within a single

bacteriophage species. Virology Journal 8:134.
Chase, T. E., J. A. Nelson, D. E. Burbank, and J. L. Van Etten. 1989. Mutual Exclusion Occurs in a *Chlorella*-like Green Alga Inoculated with Two Viruses. Journal of General Virology 70:1829–1836.
Chaturvedi, S., J. Klein, N. Vardi, C. Bolovan-Fritts, M. Wolf, K. Du, L. Mlera, M. Calvert, N. J. Moorman, F. Goodrum, B. Huang, and L. S. Weinberger. 2020. A molecular mechanism for probabilistic bet hedging and its role in viral latency. Proceedings of the National Academy of Sciences of the United States of America 117:17240–17248.
Cheng, Y. S., J. Labavitch, and J. S. VanderGheynst. 2015. Organic and Inorganic Nitrogen Impact *Chlorella variabilis* Productivity and Host Quality for Viral Production and Cell Lysis. Applied Biochemistry and Biotechnology 176:467–479.
Clasen, J. L., and J. J. Elser. 2007. The effect of host *Chlorella* NC64A carbon : phosphorus ratio on the production of *Paramecium bursaria* Chlorella Virus-1. Freshwater Biology 52:112–122.
Cottrell, M. T., and C. A. Suttle. 1995. Dynamics of a lytic virus infecting the photosynthetic marine picoflagellate *Micromonas pusilla*. Limnology and Oceanography 40:730–739.
De Paepe, M., and F. Taddei. 2006. Viruses' life history: towards a mechanistic basis of a trade-off between survival and reproduction among phages. PLOS Biology 4:e193.
Delbrück, M. 1945. The burst size distribution in the growth of bacterial viruses (bacteriophages). Journal of Bacteriology 50:131–135.
DeLong, J. P., Z. Al-Ameeli, G. Duncan, J. L. Van Etten, and D. D. Dunigan. 2016. Predators catalyze an increase in chloroviruses by foraging on the symbiotic hosts of zoochlorellae. Proceedings of the National Academy of Sciences of the United States of America 113:13780–13784.
DeLong, J. P., Z. Al-Ameeli, S. Lyon, J. L. Van Etten, and D. D. Dunigan. 2018. Size-dependent catalysis of chlorovirus population growth by a messy feeding predator. Microbial Ecology 75:847–853.
DeLong, J. P., M. A. Al-Sammak, Z. T. Al-Ameeli, D. D. Dunigan, K. F. Edwards, J. J. Fuhrmann, J. P. Gleghorn, H. Li, K. Haramoto, A. O. Harrison, M. F. Marston, R. M. Moore, S. W. Polson, B. D. Ferrell, M. E. Salsbery, C. R. Schvarcz, J. Shirazi, G. F. Steward, J. L. Van Etten, and K. E. Wommack. 2022. Towards an integrative view of virus phenotypes. Nature Reviews Microbiology 20:83–94.
Demory, D., L. Arsenieff, N. Simon, C. Six, F. Rigaut-Jalabert, D. Marie, P. Ge, E. Bigeard, S. Jacquet, A. Sciandra, O. Bernard, S. Rabouille, and A.-C. Baudoux. 2017. Temperature is a key factor in *Micromonas*-virus interactions. ISME Journal 11:601–612.
Demory, D., R. Liu, Y. Chen, F. Zhao, A. R. Coenen, Q. Zeng, and J. S. Weitz. 2021a. Linking Light-Dependent Life History Traits with Population Dynamics for *Prochlorococcus* and Cyanophage. mSystems 5:e00586-19.
Demory, D., J. S. Weitz, A.-C. Baudoux, S. Touzeau, N. Simon, S. Rabouille, A. Sciandra, and O. Bernard. 2021b. A thermal trade-off between viral production and degradation drives virus-phytoplankton population dynamics. Ecology Letters 24:1133–1144.
Dessau, M., D. Goldhill, R. L. McBride, P. E. Turner, and Y. Modis. 2012. Selective Pressure Causes an RNA Virus to Trade Reproductive Fitness for Increased Structural and Thermal Stability of a Viral Enzyme. PLoS Genetics 8.
Dunigan, D. D., R. L. Cerny, A. T. Bauman, J. C. Roach, L. C. Lane, I. V. Agarkova, K. Wulser, G. M. Yanai-Balser, J. R. Gurnon, J. C. Vitek, B. J. Kronschnabel, A. Jeanniard, G. Blanc, C. Upton, G. A. Duncan, O. W. McClung, F. Ma, and J. L. Van Etten. 2012. *Paramecium bursaria* Chlorella Virus 1 Proteome Reveals Novel Architectural and Regulatory Features of a Giant Virus. Journal of Virology 86:8821–8834.
Edwards, K. F., and G. F. Steward. 2018. Host Traits Drive Viral Life Histories across Phytoplankton Viruses. American Naturalist 191:566–581.
Edwards, K. F., G. F. Steward, and C. R. Schvarcz. 2021. Making sense of virus size and the tradeoffs shaping viral fitness. Ecology Letters 24:363–373.

Erez, Z., I. Steinberger-Levy, M. Shamir, S. Doron, A. Stokar-Avihail, Y. Peleg, S. Melamed, A. Leavitt, A. Savidor, S. Albeck, G. Amitai, and R. Sorek. 2017. Communication between viruses guides lysis-lysogeny decisions. Nature 541:488–493.
Frank, S. A. 1996. Models of parasite virulence. Quarterly Review of Biology 71:37–78.
Frickel, J., M. Sieber, and L. Becks. 2016. Eco-evolutionary dynamics in a co-evolving host-virus system. Ecology Letters 19:450–459.
Frohns, F., A. Käsmann, D. Kramer, B. Schäfer, M. Mehmel, M. Kang, J. L. Van Etten, S. Gazzarrini, A. Moroni, and G. Thiel. 2006. Potassium Ion Channels of *Chlorella* Viruses Cause Rapid Depolarization of Host Cells during Infection. Journal of Virology 80:2437–2444.
Frois-Moniz, K. 2014. Host/virus interactions in the marine cyanobacterium *Prochlorococcus*. Thesis, Massachusetts Institute of Technology.
Furió, V., A. Moya, and R. Sanjuán. 2005. The cost of replication fidelity in an RNA virus. Proceedings of the National Academy of Sciences of the United States of America 102:10233–10237.
Gallet, R., T. Lenormand, and I. N. Wang. 2012. Phenotypic Stochasticity Protects Lytic Bacteriophage Populations From Extinction During The Bacterial Stationary Phase. Evolution 66:3485–3494.
García-Villada, L., and J. W. Drake. 2013. Experimental selection reveals a trade-off between fecundity and lifespan in the coliphage Qß. Open Biology 3:130043.
Garland, T. Jr., A. W. Dickerman, C. M. Janis, and J. A. Jones. 1993. Phylogenetic analysis of covariance by computer simulation. Systematic Biology 42:265–292.
Garza, D. R., and C. A. Suttle. 1998. The Effect of Cyanophages on the Mortality of *Synechococcus* spp. and Selection for UV Resistant Viral Communities. Microbial Ecology 36:281–292.
Goldhill, D. H., and P. E. Turner. 2014. The evolution of life history trade-offs in viruses. Current Opinion in Virology 8:79–84.
Graves, M. V., D. E. Burbank, R. Roth, J. Heuser, P. L. DeAngelis, and J. L. Van Etten. 1999. Hyaluronan synthesis in virus PBCV-1-infected chlorella-like green algae. Virology 257:15–23.
Greiner, T., F. Frohns, M. Kang, J. L. Van Etten, A. Käsmann, A. Moroni, B. Hertel, and G. Thiel. 2009. *Chlorella* viruses prevent multiple infections by depolarizing the host membrane. Journal of General Virology 90:2033–2039.
Hall, M. D., G. Bento, and D. Ebert. 2017. The evolutionary consequences of stepwise infection processes. Trends in Ecology & Evolution 32:612–623.
Heineman, R. H., and S. P. Brown. 2012. Experimental Evolution of a Bacteriophage Virus Reveals the Trajectory of Adaptation across a Fecundity/Longevity Trade-Off. PLoS ONE 7.
Heineman, R. H., and J. J. Bull. 2007. Testing optimality with experimental evolution: Lysis time in a bacteriophage. Evolution 61:1695–1709.
Hiatt, C. W. 1964. Kinetics of the inactivation of viruses. Bacteriological Reviews 28:150–163.
Holm, S. 1979. A simple sequentially rejective multiple test procedure. Scandinavian Journal of Statistics 6:65–70.
Horas, E. L., L. Theodosiou, and L. Becks. 2018. Why Are Algal Viruses Not Always Successful? Viruses 10:474.
Hyman, P., and S. T. Abedon. 2009. Practical Methods for Determining Phage Growth Parameters. Pages 175–202 *in* M. R. J. Clokie and A. M. Kropinski, editors. Bacteriophages: Methods and Protocols, Volume 1: Isolation, Characterization, and Interactions, vol. 401. Humana Press.
Jeanniard, A., D. D. Dunigan, J. R. Gurnon, I. V. Agarkova, M. Kang, J. Vitek, G. Duncan, O. W. McClung, M. Larsen, J. M. Claverie, J. L. Van Etten, and G. Blanc. 2013. Towards defining the chloroviruses: A genomic journey through a genus of large DNA viruses. BMC Genomics 14.
Jurczak-Kurek, A., T. Gąsior, B. Nejman-Faleńczyk, S. Bloch, A. Dydecka, G. Topka, A. Necel, M. Jakubowska-Deredas, M. Narajczyk, M. Richert, A. Mieszkowska, B. Wróbel, G. Węgrzyn, and A. Węgrzyn. 2016. Biodiversity of bacteriophages: Morphological and biological properties of a large group of phages isolated from urban sewage. Scientific Reports 6:1–17.
Kahn Mirzaei, M., and A. S. Nilsson. 2015. Isolation of Phages for Phage Therapy: A Comparison of Spot Tests and Efficiency of Plating Analyses for Determination of Host Range and Efficacy.

PloS ONE 10:e0118557.
Kawasaki, T., M. Tanaka, M. Fujie, S. Usami, K. Sakai, and T. Yamada. 2002. Chitin synthesis in chlorovirus CVK2-infected chlorella cells. Virology 302:123–131.
Keen, E. C. 2014. Tradeoffs in bacteriophage life histories. Bacteriophage 4:e28365.
Klasse, P. J. 2015. Molecular Determinants of the Ratio of Inert to Infectious Virus Particles. Progress in Molecular Biology and Translational Science 129:285–326.
Koch, G. 1960. Influence of assay conditions on infectivity of heated poliovirus. Virology 12:601–603.
Kukkaro, P., and D. H. Bamford. 2009. Virus–host interactions in environments with a wide range of ionic strengths. Environmental Microbiology Reports 1:71–77.
Leggett, H. C., R. Benmayor, D. J. Hodgson, and A. Buckling. 2013. Experimental evolution of adaptive phenotypic plasticity in a parasite. Current Biology 23:139–142.
Lievens, E. J. P. 2022a. Virion quantification by flow cytometry, without fixation or freezing. dx.doi.org/10.17504/protocols.io.6qpvr6q93vmk/v1.
Lievens, E. J. P. 2022b. Modified one-step growth (mOSG) assay. dx.doi.org/10.17504/protocols.io.4r3l2op9pv1y/v2.
Lievens, E. J. P. 2022c. Modified persistence (mP) assay. dx.doi.org/10.17504/protocols.io.81wgb6knylpk/v2.
Lievens, E. J. P., M. Spagnuolo, T. Réveillon, and L. Becks. 2022. Delayed lysis time at high multiplicities of particles in a chlorovirus-*Chlorella* interaction. Microbes and Environments 37:ME22068.
Lippé, R. 2018. Flow Virometry: a Powerful Tool To Functionally Characterize Viruses. Journal of Virology 92:e01765-17.
Litt, P. K., and D. Jaroni. 2017. Isolation and Physiomorphological Characterization of *Escherichia coli* O157:H7-Infecting Bacteriophages Recovered from Beef Cattle Operations. International Journal of Microbiology 2017:e7013236.
Long, A. M., and S. M. Short. 2016. Seasonal determinations of algal virus decay rates reveal overwintering in a temperate freshwater pond. ISME Journal 10:1602–1612.
Maat, D. S., and C. P. D. Brussaard. 2016. Both phosphorus- and nitrogen limitation constrain viral proliferation in marine phytoplankton. Aquatic Microbial Ecology 77:87–97.
Meints, R. H., D. E. Burbank, J. L. Van Etten, and D. T. A. Lamport. 1988. Properties of the chlorella receptor for the virus PBCV-1. Virology 164:15–21.
Meints, R. H., K. Lee, and J. L. Van Etten. 1986. Assembly site of the virus PBCV-1 in a *Chlorella*-like green alga: ultrastructural studies. Virology 154:240–245.
Millard, S. P. 2013. EnvStats: An R Package for Environmental Statistics. Springer, New York.
Milrot, E., E. Shimoni, T. Dadosh, K. Rechav, T. Unger, J. L. Van Etten, and A. Minsky. 2017. Structural studies demonstrating a bacteriophage-like replication cycle of the eukaryote-infecting *Paramecium bursaria* chlorella virus-1. PLOS Pathogens 13:e1006562.
Mojica, K. D. A., and C. P. D. Brussaard. 2014. Factors affecting virus dynamics and microbial host–virus interactions in marine environments. FEMS Microbiology Ecology 89:495–515.
Nakagawa, S., and H. Schielzeth. 2010. Repeatability for Gaussian and non-Gaussian data: a practical guide for biologists. Biological Reviews 85:935–956.
Nichols, H. W., and H. C. Bold. 1965. *Trichosarcina polymorpha* Gen. et Sp. Nov. Journal of Phycology 1:34–38.
Pasek, J. 2021. weights: Weighting and Weighted Statistics, version 1.0.4.
Pinon, A., and M. Vialette. 2018. Survival of viruses in water. Intervirology 61:214–222.
Quispe, C. F., A. Esmael, O. Sonderman, M. McQuinn, I. Agarkova, M. Battah, G. A. Duncan, D. D. Dunigan, P. L. Timothy, C. DeCastro, I. Speciale, F. Ma, and J. L. Van Etten. 2017. Characterization of a New Chlorovirus Type with Permissive and Non-permissive Features on Phylogenetically Related Algal Strains. Virology 500:103–113.
Quispe, C. F., O. Sonderman, A. Seng, B. Rasmussen, G. Weber, C. Mueller, D. D. Dunigan, and J. L. Van Etten. 2016. Three-year survey of abundance, prevalence and genetic diversity of chlorovirus

populations in a small urban lake. Archives of Virology 161:1839–1847.
R Core Team. 2014. R: A language and environment for statistical computing. R Foundation for Statistical Computing, Vienna, Austria.
Record, N. R., D. Talmy, and S. Våge. 2016. Quantifying tradeoffs for marine viruses. Frontiers in Marine Science 3:251.
Rodrigues, R. A. L., V. F. Queiroz, J. Ghosh, D. D. Dunigan, and J. L. Van Etten. 2022. Functional Genomic Analyses Reveal an Open Pan-genome for the Chloroviruses and a Potential for Genetic Innovation in New Isolates. Journal of Virology 96:e01367-21.
Rowe, J. M., D. D. Dunigan, G. Blanc, J. R. Gurnon, Y. Xia, and J. L. Van Etten. 2013. Evaluation of higher plant virus resistance genes in the green alga, *Chlorella variabilis* NC64A, during the early phase of infection with *Paramecium bursaria* chlorella virus-1. Virology 442:101–113.
Roy, D., E. S. K. Chian, and R. S. Engelbrecht. 1982. Mathematical model for enterovirus inactivation by ozone. Water Research 16:667–673.
Schiano di Visconte, G., M. J. Allen, and A. Spicer. 2022. New Insights from the High-Resolution Monitoring of Microalgae–Virus Infection Dynamics. Viruses 14:466.
Stearns, S. C. 1989. Trade-Offs in Life-History Evolution. Functional Ecology 3:259–268.
Stenholm, A. R. nnest, I. Dalsgaard, and M. Middelboe. 2008. Isolation and Characterization of Bacteriophages Infecting the Fish Pathogen *Flavobacterium psychrophilum*. Applied and Environmental Microbiology 74:4070–4078.
Šulčius, S., E. Šimoliūnas, J. Staniulis, J. Koreivienė, P. Baltrušis, R. Meškys, and R. Paškauskas. 2015. Characterization of a lytic cyanophage that infects the bloom-forming cyanobacterium *Aphanizomenon flos-aquae*. FEMS Microbiology Ecology 91:1–7.
Suttle, C. A. 2007. Marine viruses - Major players in the global ecosystem. Nature Reviews Microbiology 5:801–812.
Suttle, C. A., and A. M. Chan. 1994. Dynamics and distribution of cyanophages and their effect on marine *Synechococcus* spp. Applied and Environmental Microbiology 60:3167–3174.
Swihart, B., and J. Lindsey. 2019. gnlm: Generalized Nonlinear Regression Models, version 1.1.1.
Taylor, B. P., J. S. Weitz, C. P. D. Brussaard, and M. G. Fischer. 2018. Quantitative Infection Dynamics of *Cafeteria Roenbergensis* Virus. Viruses 10:468.
Tessman, I. 1985. Genetic recombination of the DNA plant virus PBCV1 in a *Chlorella*-like alga. Virology 145:319–322.
Thiel, G., A. Moroni, D. D. Dunigan, and J. L. Van Etten. 2010. Initial Events Associated with Virus PBCV-1 Infection of *Chlorella* NC64A. Progress in Botany 71:169–183.
Timm, A., and J. Yin. 2012. Kinetics of virus production from single cells. Virology 424:11–17.
Tomaru, Y., H. Tanabe, S. Yamanaka, and K. Nagasaki. 2005. Effects of temperature and light on stability of microalgal viruses, HaV, HcV and HcRNAV. Plankton Biology and Ecology 52:1–6.
Tseng, M., and J. H. Myers. 2014. The relationship between parasite fitness and host condition in an insect -virus system. PLoS ONE 9:e106401.
Van Etten, J. L., I. V. Agarkova, and D. D. Dunigan. 2020. Chloroviruses. Viruses 12:20.
Van Etten, J. L., D. E. Burbank, Y. Xia, and R. H. Meints. 1983. Growth cycle of a virus, PBCV-1, that infects *Chlorella*-like algae. Virology 126:117–125.
Van Etten, J. L., A. M. Schuster, and R. H. Meints. 1988. Viruses of eukaryotic *Chlorella*-like algae. Pages 411–428 *in* Y. Koltin and M. J. Leibowitz, editors. Viruses of Fungi and Simple Eukaryotes. Marcel Dek. New York and Basel.
Wang, I.-N. 2006. Lysis Timing and Bacteriophage Fitness. Genetics 172:17–26.
Weitz, J. 2016. Quantitative Viral Ecology: Dynamics of Viruses and Their Microbial Hosts. Princeton University Press.
Wen, K., A. C. Ortmann, and C. A. Suttle. 2004. Accurate estimation of viral abundance by epifluorescence microscopy. Applied and Environmental Microbiology 70:3862–3867.
Wood, S. N. 2017. Generalized Additive Models: An Introduction with R. Second edition. Chapman and Hall/CRC.

Yan, X., N. H. Olson, J. L. Van Etten, M. Bergoin, M. G. Rossmann, and T. S. Baker. 2000. Structure and assembly of large lipid-containing dsDNA viruses. Nature Structural Biology 7:101–103.
Zaburlin, D., A. Quiberoni, and D. Mercanti. 2017. Changes in Environmental Conditions Modify Infection Kinetics of Dairy Phages. Food and Environmental Virology 9:270–276.
Zago, M., B. Bonvini, L. Rossetti, A. Meucci, G. Giraffa, and D. Carminati. 2015. Biodiversity of *Lactobacillus helveticus* bacteriophages isolated from cheese whey starters. Journal of Dairy Research 82:242–247.
Zera, A. J., and L. G. Harshman. 2001. The Physiology of Life History Trade-Offs in Animals. Annual Review of Ecological Systems 32:95–126.

## Tables

**Table 1. Definitions used in this paper.**

| Term | Our definition | Ratio to host cells |
|---|---|---|
| Virions | Virus particles that can be detected by flow cytometry (excludes e.g.DNA-free capsids[1]). | Multiplicity of particles (MOP) |
| Adsorbed virions | Virions that are adsorbed to a host cell. Virions that have not adsorbed may be incapable or may have failed to adsorb by chance. | Multiplicity of adsorption (MOA)[2] |
| Depolarizing-capable virions | Virions that can depolarize a host cell if they adsorb to one. We assume that chance plays no role in depolarization success: failure to depolarize after adsorption is always due to incapability or mutual exclusion (the cell has already been depolarized by another depolarizing-capable virion[3]). | - |
| Infectious virions | Virions that can catalyze the death of an algal population, i.e. finish a life cycle and spread to other cells. Non-infectious virions can be incapable of adsorbing, depolarizing the host[1,4], or completing the infection[5]. | Multiplicity of infection (MOI) |

[1](Agarkova et al. 2014), [2](Hyman and Abedon 2009), [3](Greiner et al. 2009), [4](Frohns et al. 2006), [5](Quispe et al. 2017)

**Table 2. List of viral strains.** We used two lysates of reference strain AR158; lysate AR158[1] was seven years older than AR158[2]. Phylogenetic positions based on Quispe et al. (2017) and Rodrigues et al. (2022).

| Group | Clade | Strains |
|---|---|---|
| NC64A viruses | PBCV-1 clade | AN69C, CV-K1 (= CviKI), CvsA1, IL-3A, KS-1B, MA-1E, NE-JV-4, PBCV-1 |
| | NY-2A clade | AR158[1], AR158[2], IL-5-2s1, MA-1D, NY-2A, NY-2B, NYs-1 |
| | unknown | CA-4A, SH-6A, WNE-10B-L2, WNE-11A-L2 (= WNE-11A-L1), XZ-4A |
| Osy viruses | Osy clade | OSyNE-5 |
| | unknown | OSyNE-4B-L2, OSyNE-4B-M2, OSyNE-4B-S2, OSyNE-5B-M2, OSyNE-5B-S1, OSyNE-ZA-1 |
| SAG viruses | SAG clade | Canal-1, GM0701.1, MN0810.1, MO0605SPH, NTS-1, TN603.4.2 |
| | unknown | NES-4A-S1, NES-5A-L1 |

**Table 3. List of life history traits.**

| Model | Parameter | Trait |
|---|---|---|
| Eq. 1 | $k$ | adsorption constant[1] |
| Eq. 1 | $d$ | depolarization probability (probability that a virion is depolarizing-capable) |
| Eq. 3 | $c$ | completion probability (probability that a depolarized cell lyses and produces progeny virions) |
| Eq. 1 | $\alpha$ (set to 0) | truncation value of lysis time (earliest possible lysis time) |
| Eq. 1 | $\mu_l$ | mean lysis time |
| Eq. 1 | $\sigma_l$ | standard deviation of lysis time |
| Eq. 1 | $b_d$ | average burst size per depolarized cell |
| Eq. 4 | $b_c$ | average burst size per completed cell |
| Eq. 2 | $s$ | specific infectivity (proportion of virions that are infectious when the solution is fresh) |
| Eq. 2 | $r$ | robust fraction (fraction of initially infectious virions that do not decay within the timeframe of the mP assay) |

| | | |
|---|---|---|
| Eq. 2 | *m* | mortality rate of the fragile infectious virions |

[1](Hyman and Abedon 2009)

**Table 4. Additional correlations that we hypothesized could occur between traits, based on trade-offs found in or suggested by the literature.**

| Trade-off | Expected correlations | Basis |
|---|---|---|
| Short-term vs. long-term virion quality | - positive correlation between specific infectivity *s* and mortality rate *m*<br>- negative correlation between specific infectivity *s* and robust fraction *r* | Reflection of the general expectation that trade-offs occur between adaptations to different environments[1], in this case short-term and long-term environmental conditions. |
| Survival vs. reproduction | - positive correlation between mortality rate *m* and observed growth rate | Classic trade-off[3] that is also expected to apply to viruses[2,3,4]. |
| Offspring quantity & quality | - negative correlation between burst size per depolarised (i.e. per infected) cell $b_d$ and specific infectivity *s* | Version of the classic quantity/quality trade-off[4,5], but at $t = 0$. Related to the speed-fidelity trade-off[6,7], though other processes than mutation may cause defective virions. |
| Lysis time & burst size | - negative correlation between burst size per depolarised (i.e. per infected) cell $b_d$ and mean lysis time $\mu_l$ | Classic trade-off for lytic viruses[3], based on the assumption that progeny virions are produced until lysis occurs. |

[1](Agrawal et al. 2010), [2](De Paepe and Taddei 2006), [3](Goldhill and Turner 2014), [4](Keen 2014), [5](Stearns 1989), [6](Furió et al. 2005), [7](Belshaw et al. 2008)

## Figures

**Fig. 1. Life cycle of the chloroviruses, as assumed in our statistical models.** See the text and Table 3 for definitions of the traits. Traits marked in blue describe independent life cycle steps; traits marked in red arise from combinations of two or more steps (see gray box). Traits in bold are estimated from the modified one-step growth (mOSG) or modified persistence (mP) assays; traits not in bold are derived from comparing the two assays. Abbreviations: F, frequency when the virion solution is fresh; P, probability; "*TrN*", truncated normal distribution.

**Fig. 2. Design of a classical vs. modified one-step growth (mOSG) assay.** See the text for a description. Only one replicate is shown for the classical assay. Abbreviations: $b$, burst size; $b_d$, burst size per depolarized cell; $d$, depolarization probability; $k$, adsorption constant; $l$, lysis time; PFU, plaque-forming unit; $t$, time; $t_a$, adsorption time.

**Fig. 3. Design of a classical vs. modified persistence (mP) assay.** See the text for a description. Only one replicate is shown for the classical assay. Abbreviations: $m$, mortality rate; MPN, most probable number; $s$, specific infectivity; $t$, time.

**Fig. 4. Trait diversity within and among chlorovirus groups. Upper panels: Trait estimates and 95 % CIs**. Estimates and CIs colored in black were retained for further analysis; estimates and traits colored red were excluded from the analyses due to poor or imprecise model fit. Note that precision should be evaluated by comparing the CI breadth to the plausible phenotypic range, not the x-axis scale (particularly for $s$ and $m$). Missing traits are due to failed or incomplete assays. See Supp. Table S1 for details and exact values. **Lower panels: Distributions of the retained estimates.** Shown as violin plots with internal box plots. Only the estimates used in the analyses are included in these distributions (i.e. those shown in black in the upper panels). Abbreviations: "comp.", completed; "depol.", depolarized; "prob.", probability.

**Fig. 5. Analyses of viral growth.** Virus strains are colored by group: NC64A viruses in blue, SAG viruses in red, Osy viruses in gold. For the NC64A viruses, darker shades indicate faster-growing strains. **A.** Variation in relative growth among strains. **B.** Observed vs. predicted growth rate (significant correlation marked with a star). The line is the 1:1 line. **C.** Observed growth rate vs. specific infectivity $s$. Open points represent strains for which only $s$, $k$, and genome size were known; solid points represent strains with known $s$, $k$, $\mu_l$, $b_c$, and genome size. The dashed line shows the predictions of the best model for the unrestricted dataset (only $s$, $k$, and genome size analyzed), which showed that growth rate was best explained by $s$.

**Fig. 6. Correlations between traits in the NC64A viruses.** Each point represents one virus strain; darker shades indicate faster-growing strains (see Fig. 5A). Panels with significant Spearman correlations are marked with stars. Analyses were weighted by the estimates' CI breadth; a version of these panels with 95 % CIs can be found in Supp. Fig. S13. Abbreviations: "depol.", depolarized.

**Supplementary Material**

Detailed legends provided in each file.

**Supp. Method S1. Derivation of Eqs. 1 & 2.**

**Supp. Table S1. Trait table for the chloroviruses, including selected traits from the literature and the traits estimated in this manuscript.**

**Supp. Table S2. ANOVA tables partitioning the trait variance within and among chlorovirus groups.**

**Supp. Table S3. Results of the regression models for observed growth rate.**

**Supp. Table S4. Correlations between traits in the NC64A virus group.**

**Supp. Fig. S1. Example of statistical fitting for the mOSG model.**

**Supp. Fig. S2. Schematic representation of the mOSG and mP protocols for one virus strain.**

**Supp. Fig. S3. Effect of imposing $\alpha$ = 0 in the mOSG model.**

**Supp. Fig. S4. Sensitivity of the mOSG model to its parameters.**

**Supp. Fig. S5. Correlations between model parameters arising from the fitting process.**

**Supp. Fig. S6. Comparing the trait estimates from Eqs. 1 & 2 to 'classical' calculations.**

**Supp. Fig. S7. Repeatability of the mOSG assay.**

**Supp. Fig. S8. Effect of imposing *r* = 0 in the mP model.**

**Supp. Fig. S9. Sensitivity of the mP model to its parameters.**

**Supp. Fig. S10. Example of statistical fitting for the mP model.**

**Supp. Fig. S11. Repeatability of the mP assay.**

**Supp. Fig. S12. Effect of correlations between model parameters arising from the fitting process.**

**Supp. Fig. S13. Correlations between traits in the NC64A viruses, with 95 % CIs.**

**Supp. Fig. S14. Exploration of the assumption that mOSG parameters are independent of MOP.**

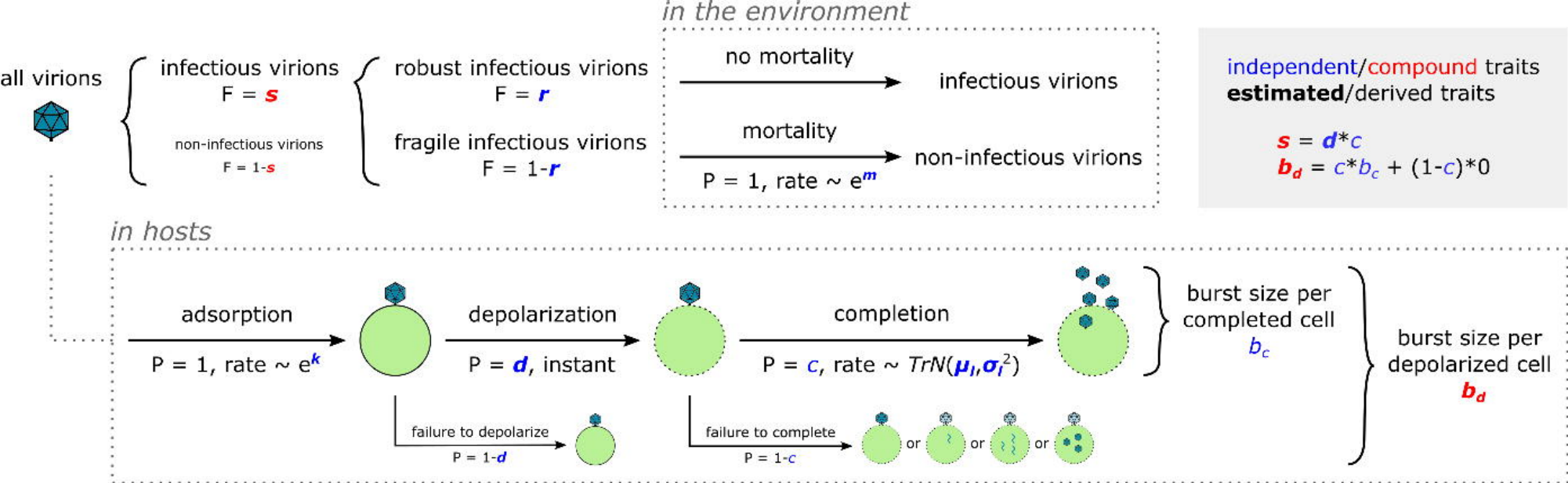
in the environment
all virions
infectious virions
F = s
non-infectious virions
F = 1-s
robust infectious virions
F = r
fragile infectious virions
F = 1-r
no mortality
infectious virions
mortality
P = 1, rate ~ e^m
non-infectious virions
independent/compound traits
estimated/derived traits
s = d*c
b_d = c*b_c + (1-c)*0
in hosts
adsorption
P = 1, rate ~ e^k
depolarization
P = d, instant
completion
P = c, rate ~ TrN(μ_l,σ_l^2)
burst size per completed cell
b_c
burst size per depolarized cell
b_d
failure to depolarize
P = 1-d
failure to complete
P = 1-c
or
or
or

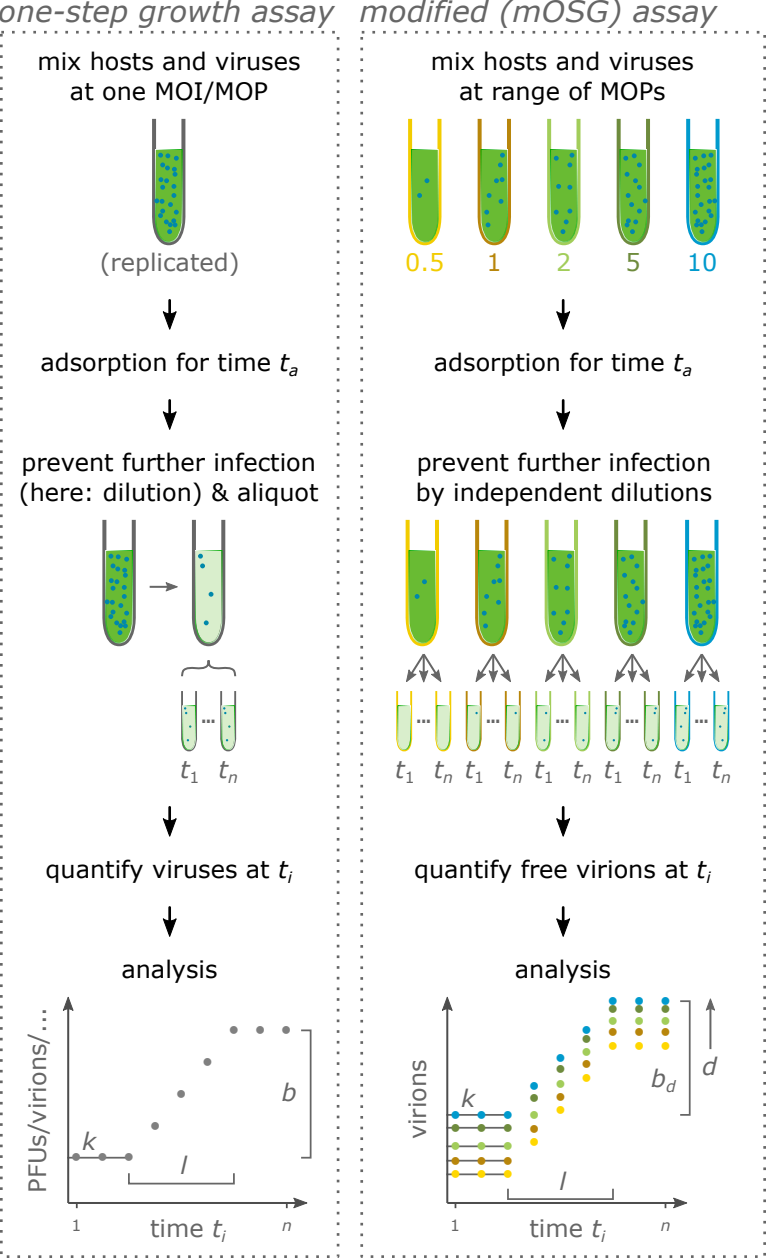
one-step growth assay
modified (mOSG) assay
mix hosts and viruses at one MOI/MOP
(replicated)
adsorption for time $t_a$
prevent further infection (here: dilution) & aliquot
$t_1$ $t_n$
quantify viruses at $t_i$
analysis
PFUs/virions/...
k
l
b
1
time $t_i$
n
mix hosts and viruses at range of MOPs
0.5
1
2
5
10
adsorption for time $t_a$
prevent further infection by independent dilutions
$t_1$ $t_n$ $t_1$ $t_n$ $t_1$ $t_n$ $t_1$ $t_n$ $t_1$ $t_n$
quantify free virions at $t_i$
analysis
virions
k
l
$b_d$
d
1
time $t_i$
n

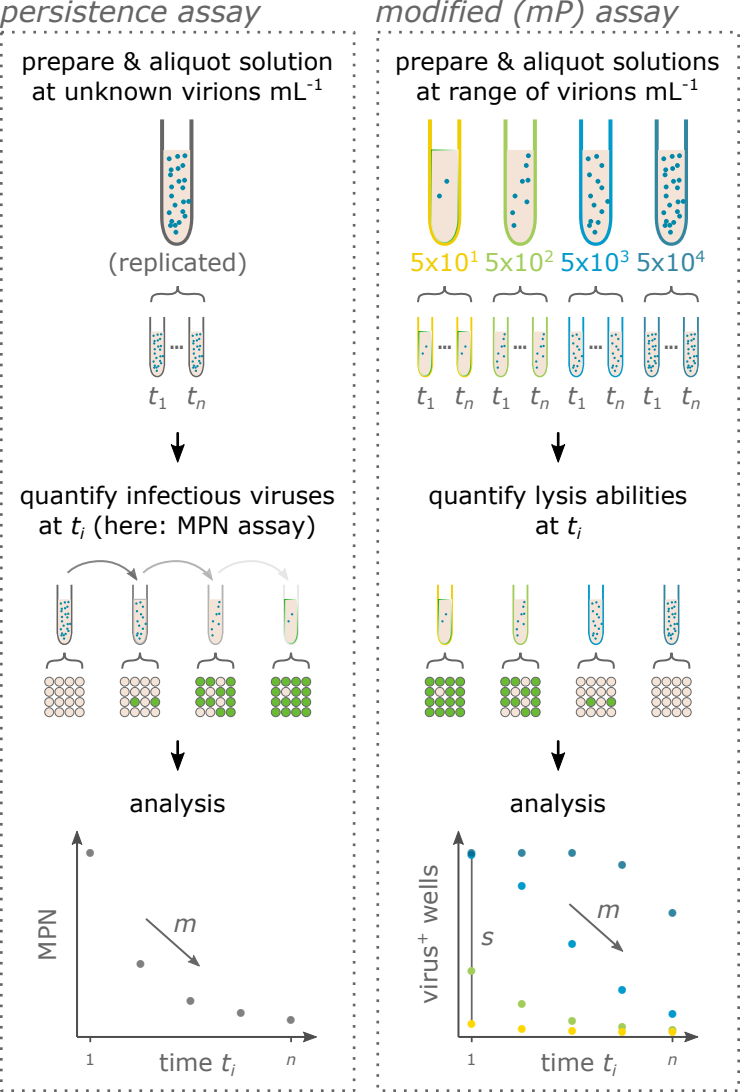
persistence assay
modified (mP) assay
prepare & aliquot solution at unknown virions mL-1
(replicated)
t1 tn
quantify infectious viruses at ti (here: MPN assay)
analysis
MPN
m
1
time ti
n
prepare & aliquot solutions at range of virions mL-1
5x10^1 5x10^2 5x10^3 5x10^4
t1 tn t1 tn t1 tn t1 tn
quantify lysis abilities at ti
analysis
virus+ wells
s
m
1
time ti
n

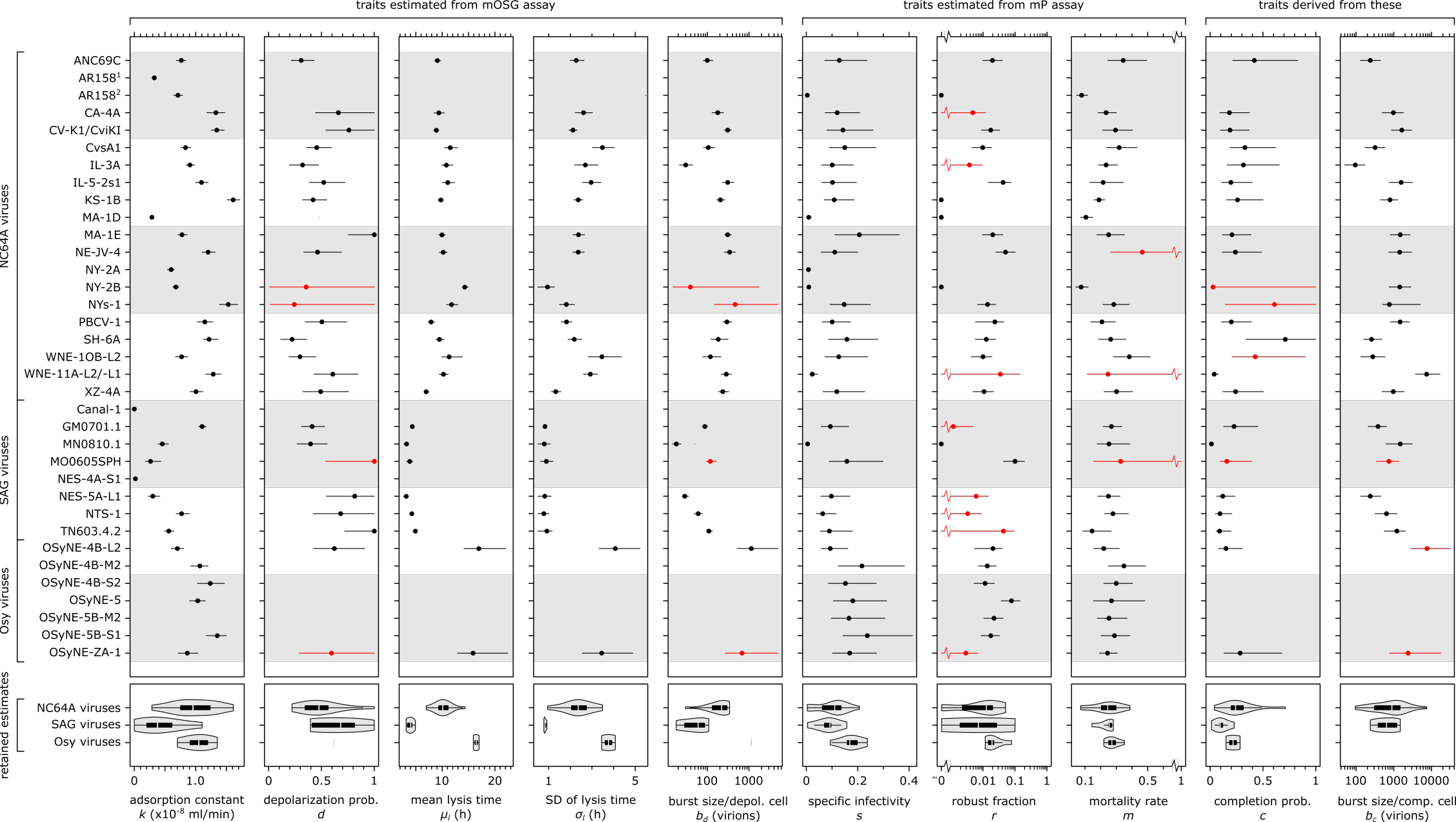
traits estimated from mOSG assay
traits estimated from mP assay
traits derived from these
NC64A viruses
SAG viruses
Osy viruses
ANC69C
AR158[1]
AR158[2]
CA-4A
CV-K1/CviKI
CvsA1
IL-3A
IL-5-2s1
KS-1B
MA-1D
MA-1E
NE-JV-4
NY-2A
NY-2B
NYs-1
PBCV-1
SH-6A
WNE-1OB-L2
WNE-11A-L2/-L1
XZ-4A
Canal-1
GM0701.1
MN0810.1
MO0605SPH
NES-4A-S1
NES-5A-L1
NTS-1
TN603.4.2
OSyNE-4B-L2
OSyNE-4B-M2
OSyNE-4B-S2
OSyNE-5
OSyNE-5B-M2
OSyNE-5B-S1
OSyNE-ZA-1
retained estimates
NC64A viruses
SAG viruses
Osy viruses
0 1.0
0 0.5 1
10 20
1 5
100 1000
0 0.2 0.4
~0 0.01 0.1 1
0.1 0.5 1
0 0.5 1
100 1000 10000
adsorption constant
k (x10-8 ml/min)
depolarization prob.
d
mean lysis time
μl (h)
SD of lysis time
σl (h)
burst size/depol. cell
bd (virions)
specific infectivity
s
robust fraction
r
mortality rate
m
completion prob.
c
burst size/comp. cell
bc (virions)

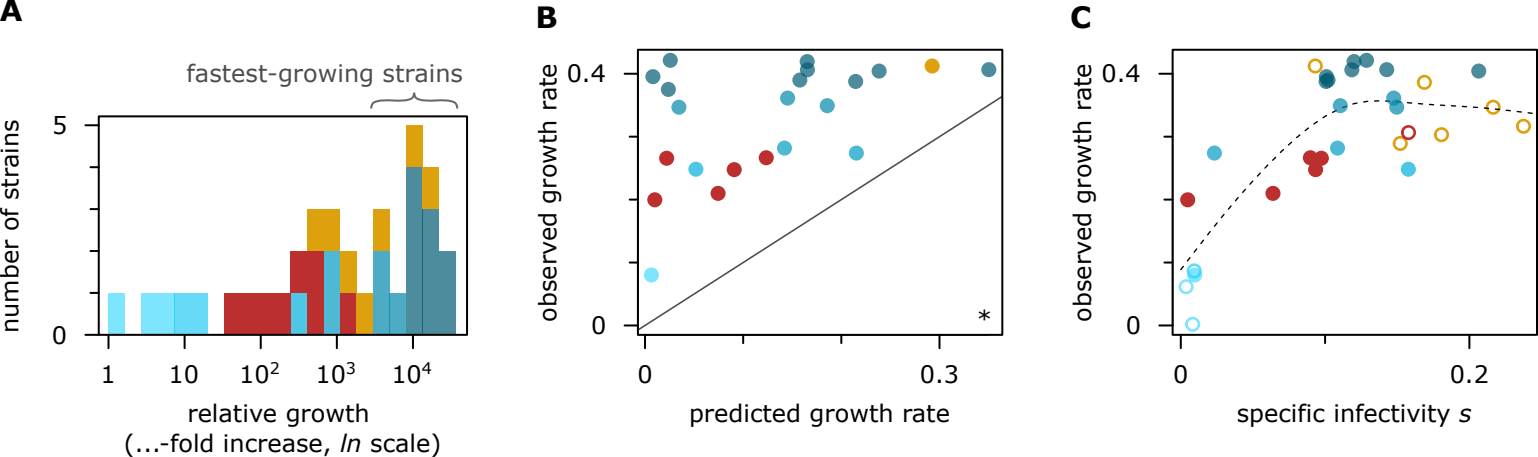
A
fastest-growing strains
number of strains
5
0
1
10
$10^2$
$10^3$
$10^4$
relative growth
(...-fold increase, *ln* scale)
B
observed growth rate
0.4
0
0
0.3
predicted growth rate
*
C
observed growth rate
0.4
0
0
0.2
specific infectivity *s*

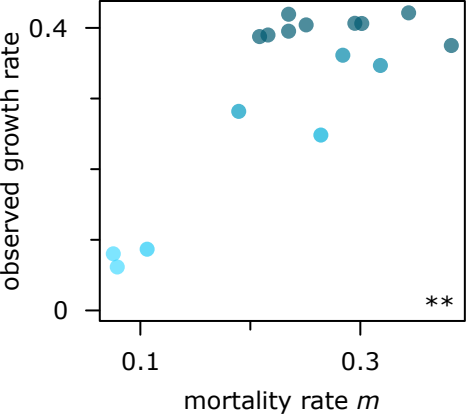
observed growth rate
0.4
0
**
0.1
0.3
mortality rate $m$

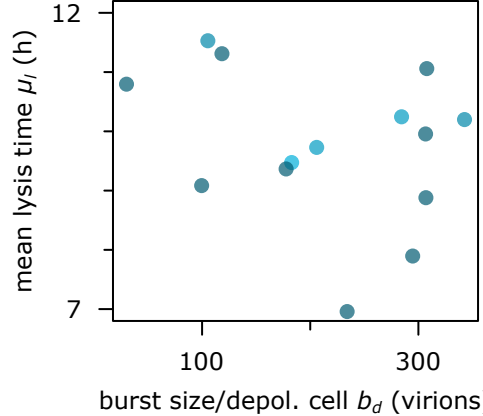
mean lysis time $\mu_l$ (h)
12
7
100
300
burst size/depol. cell $b_d$ (virions)

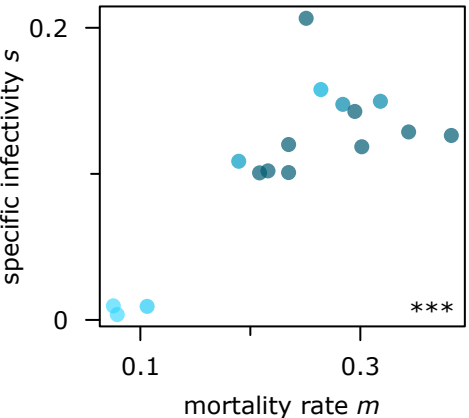
specific infectivity $s$
0.2
0
***
0.1
0.3
mortality rate $m$

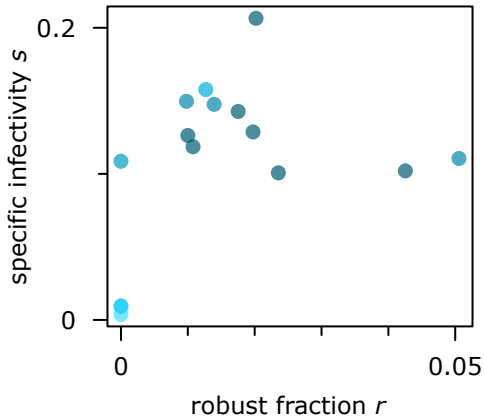
specific infectivity $s$
0.2
0
0
0.05
robust fraction $r$

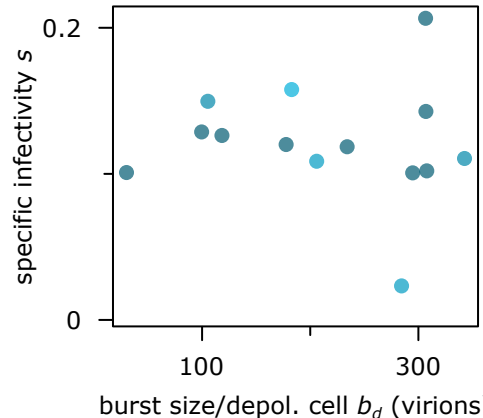
specific infectivity $s$
0.2
0
100
300
burst size/depol. cell $b_d$ (virions)